Schweizerische Eidgenossenschaft
Confédération suisse
Confederazione Svizzera
Confederaziun svizra

Eidgenössisches Departement für Umwelt, Verkehr, Energie und Kommunikation UVEK

Bundesamt für Energie BFE
Sektion Energieforschung

Schlussbericht 15.12.2017

Einfluss des Sedimenttransports durch Umleitstollen auf die Hydroabrasion der Stollensohle und auf die Ökomorphologie im Unterwasser

ETH zürich

Versuchsanstalt für Wasserbau,
Hydrologie und Glaziologie

Datum: 15.12.2017

Ort: Bern

Auftraggeberin:
Bundesamt für Energie BFE
Forschungsprogramm Wasserkraft
CH-3003 Bern
www.bfe.admin.ch

Auftragnehmerin:
ETH Zürich
Versuchsanstalt für Wasserbau, Hydrologie und Glaziologie (VAW)
Hönggerbergring 26
CH-8093 Zürich
www.vaw.ethz.ch

Autoren:
Michelle Müller-Hagmann, ETH Zürich, mueller-hagmann@vaw.baug.ethz.ch
Matteo Facchini, ETH Zürich, facchini@vaw.baug.ethz.ch
Dr. Ismail Albayrak, ETH Zürich, albayrak@vaw.baug.ethz.ch
Prof. Dr. Robert Boes, ETH Zürich, boes@vaw.baug.ethz.ch

BFE-Bereichsleitung: Dr. Michael Moser, michael.moser@bfe.admin.ch
BFE-Programmleitung: Dr. Klaus Jorde, klaus.jorde@kjconsult.net
BFE-Vertragsnummer: SI/501114-01

Bundesamt für Energie BFE
Mühlestrasse 4, CH-3063 Ittigen; Postadresse: CH-3003 Bern
Tel. +41 58 462 56 11 · Fax +41 58 463 25 00 · contact@bfe.admin.ch · www.bfe.admin.ch

Zusammenfassung

Zur nachhaltigen Bewirtschaftung von Stauanlagen ist ein umfassendes Sedimentmanagement erforderlich. Sedimentumleitstollen (*Sediment Bypass Tunnels* = SBTs) können dabei einen wichtigen Beitrag zur Wiederherstellung des gestörten Sedimenttransports leisten und so nicht nur den Stauraum vor Verlandung schützen, sondern auch die Ökomorphologie im Unterstrom signifikant verbessern. Dabei können aber Schäden durch Hydroabrasions an der SBT-Sohle auftreten und hohe Unterhaltskosten verursachen. Ziel dieses Projektes war es deshalb, mittels *in-situ* Versuchen am SBT Solis an der Albula (1) die Zusammenhänge zwischen Beanspruchung, Materialeigenschaften und Abrasionstiefen zu untersuchen, und (2) den Einfluss des SBT-Betriebs auf die Ökomorphologie im Unterwasser zu analysieren. Die Abrasion der Stollensohle wurde mittels 3D-Laser aufgenommen. Obschon visuell feststellbar, konnten die Abrasionstiefen bisher messtechnisch nicht quantifiziert werden, da sie im Bereich der Messgenauigkeit des Lasermessgeräts liegen. Eine Weiterführung des Monitorings ist daher angezeigt. Das Monitoring der Gewässerökomorphologie umfasste neben LiDAR- auch Meso-Habitats- und Sedimentaufnahmen. Die Daten der beiden LiDAR-Vermessungen und der Sedimentaufnahmen wurden aufbereitet und analysiert. Die Ergebnisse der Sedimentanalysen zeigen, dass Inbetriebnahmen des SBTs die Kornverteilung des Flussbettes rasch ändern können. Die LiDAR-Vermessungen erlauben eine detailliertere Untersuchung des Einflusses der SBT-Ereignisse auf die Morphologie.

Résumé

Pour une gestion durable des barrages une gestion globale des sédiments est nécessaire. Des tunnels de dérivation de sédiments (SBTs) peuvent apporter une contribution importante de rétablir le transport des sédiments perturbé. Par conséquence SBTs ne protègent pas seulement les réservoirs de sédimentation, mais améliorent aussi de manière significative la qualité éco-morphologique des rivières. Pourtant, des dégâts hydroabrasifs sévères peuvent nécessiter des travaux de réhabilitation coûteux. Donc, le but de ce projet était d'analyser *in-situ* dans la SBT Solis sur la rivière Albula (1) la relation entre l'impact, les propriétés des matériaux et l'hydroabrasion et (2) l'influence des opérations de SBT sur l'éco-morphologie de la rivière an aval. Les abrasions du radier ont été mesurées par 3D-Laser-Scanning. Bien que les abrasions soient déjà découvrables visuellement, il n'était pas possible de les détecter d'une manière quantitative. Par conséquent, il est prévu de continuer la surveillance. Les études éco-morphologiques comprenaient des vols LiDAR, des campagnes d'échantillonnage de sédiments et des enquêtes de méso-habitat. Les résultats suggèrent que les opérations du SBT modifient rapidement la composition granulométrique du lit de la rivière. Grâce à l'analyse des données LiDAR, une analyse quantitative des effets morphologiques des opérations de la SBT a été possible.

Abstract

For a sustainable and eco-friendly reservoir operation, long-term sediment management strategies are required. Among others, Sediment bypass tunnels (SBTs) are an effective and holistic countermeasure against reservoir sedimentation. They reduce reservoir sedimentation, restore disturbed sediment transport and thus enhance the eco-morphology of the downstream river reach. However, high flow velocities in combination with high sediment transport rates cause severe hydro-abrasive damages at the tunnel invert, resulting in expensive refurbishment works. Therefore, the present project aims at (1) addressing the hydro-abrasion problem and (2) investigating the effect of SBT operation on the eco-morphology of the downstream reach of the Albula river at the test case Solis SBT. The abrasion depths

of various invert test fields implemented in the SBT were measured using a 3D-LASER-Scanner. Although abrasion traces on the various invert materials at the SBT were visually observed, it was not possible to extract quantitative abrasion depths from the scanned surface maps due to their low extent in the order of the laser device measurement accuracy. Therefore, the monitoring will be continued in the coming years. The eco-morphological investigations included two LiDAR flights, sediment sampling campaigns and meso-habitat surveys. The results suggest that SBT operations change the riverbed grain size composition rather rapidly, and that thanks to the analysis of the LiDAR data, a quantitative analysis of the morphological effects of the SBT operations was possible.

Inhaltsverzeichnis

1. Ausgangslage

Stauanlagen stellen wichtige Ressourcen bezüglich Energiegewinnung, Wasserversorgung und Hochwasserschutz dar. Vor dem Hintergrund des angestrebten Atomausstiegs, des prognostizierten Bevölkerungswachstums und der erwarteten Zunahme von Wetterextremen gewinnen Stauanlagen zusätzlich an Bedeutung. Durch den stetigen Sedimenteintrag verlanden die Reservoire aber zusehends und können im Extremfall sogar ein Sicherheitsrisiko darstellen.

Für den sicheren und nachhaltigen Betrieb von Wasserkraftanlagen ist ein situationsspezifisches Sedimentmanagement von zentraler Bedeutung (Boes *et al.* 2014, Kondolf *et al.* 2014). Sedimentumleitstollen (*Sediment Bypass Tunnels* = SBTs) können dazu einen wichtigen Beitrag leisten. Sie leiten die Sedimente in Echtzeit um den Stauraum herum ab (Abbildung 1), stellen so die gestörte Geschiebedurchgängigkeit wieder her und reduzieren damit die Stauraumverlandung (Sumi *et al.* 2004). Das Sedimentdefizit im Unterlauf und die damit einhergehenden Probleme, wie Erosion, Verkümmerung der Morphologie und Reduktion der Habitatsqualität bis hin zu Nährstoff- und Sedimentdefiziten in Küstenregionen werden so gemindert (Syvitski *et al.* 2005, Kantoush and Sumi 2010, Fukuda *et al.* 2012, Fukuroi 2012, Kondolf *et al.* 2014, Facchini *et al.* 2015, Martin *et al.* 2015). Aufgrund der extremen Betriebsbedingungen in SBTs mit hohen Fliessgeschwindigkeiten und Sedimenttransportraten können allerdings massive Hydroabrasionschäden an der Sohle auftreten (Abbildung 2) und hohe Kosten für den Unterhalt verursachen.

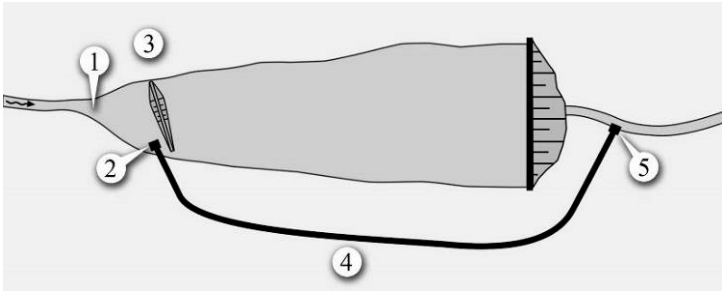

Abbildung 1: Schema eines Sedimentumleitstollens mit 1) Stauwurzel des Speichers, 2) Einlaufbauwerk, 3) Leitbauwerk, 4) Sedimentumleitstollen, 5) Auslaufbauwerk (VAW, ETH Zürich)

Abbildung 2: Mehrere Meter tief in den felsigen Untergrund reichende Abrasionsrinne im SBT Palagnedra (Baumer and Radogna 2015)

Weltweit gibt es erst wenige SBTs, weshalb die damit erzielten Nutzen wie auch verursachten Probleme noch wenig untersucht sind. Im vorliegenden Forschungsprojekt werden darum zwei zentrale Aspekte mittels Prototypversuchen am SBT der Stauanlage Solis an der Albula (Kanton Graubünden, Schweiz) untersucht: (1) die **Hydroabrasion** im SBT und (2) die Auswirkungen eines SBTs auf die **Ökomorphologie** des Gewässers.

2. Ziel der Arbeit

2.1. Hydroabrasion

Das Ziel der Hydroabrasions-Untersuchung besteht darin, die Zusammenhänge zwischen Beanspruchung (hydraulische Betriebsbedingungen und Sedimenttransport), Materialeigenschaften der Sohlauskleidung und Abrasion (Schadensarten und Ausmass) anhand von Feldversuchen zu untersuchen und zu quantifizieren. Zusätzlich soll die Abrasionsbeständigkeit unterschiedlicher Materialen untersucht und verglichen werden. Schliesslich sollen die gewonnen Erkenntnisse dazu beitragen, SBTs und andere durch Hydroabrasion beanspruchte wasserbauliche Anlagen in der Konstruktion und im Unterhalt zu optimieren und so einen Beitrag zur nachhaltigen Energie- und Wasserversorgung durch Talsperren zu leisten.

2.2. Ökomorphologie

Das Ziel des morphologischen Monitorings besteht darin, die Auswirkungen von SBT-Spülereignissen auf die unterstromige Flussmorphologie zu bewerten. Diese Effekte wurden mit neuesten Technologien wie topographische und bathymetrische Aufnahmen durch luftgestütztes Laserscanning (LiDAR) zur Erfassung der morphologischen Änderungen des Flusses Albula unterhalb der Stauanage Solis untersucht.

Die Ergebnisse dieser Untersuchung sollen schliesslich zur Optimierung des SBT-Betriebsregimes hinsichtlich Morphologie und Entlandung dienen. Die Umwelt soll nicht nur keine schädlichen Einflüsse durch den SBT-Betrieb erfahren, sondern davon profitieren.

3. Vorgehen und Methode

3.1. Hydroabrasion

Die Methodik sowie der Versuchsaufbau (Abbildung 3) bezüglich Hydroabrasion sind ausführlich im Rahmen des *Reportings* des parallel laufenden BFE Forschungsprojektes „Optimierung verschliessfester Materialien an Sedimentumleitstollen und wasserbaulichen Anlagen“ (SI/500731-01) beschrieben. Darum wird hier das Wesentliche zusammengefasst, während für detailliertere Informationen auf die Berichtserstattung zum übergeordneten Projekt verwiesen wird.

Zentrales Element dieser Untersuchung sind die sechs Testfelder, die in die Stollensohle des SBT Solis eingebaut sind (Abbildung 4). Sie sind mit unterschiedlichen Betonen, einer Schmelzbasaltpflästerung und einer Stahlpanzerung ausgestattet (siehe Jahresbericht 2015). Das Monitoring umfasst neben den sechs Testfeldern zusätzlich ein 10 m langes Stück der normalen Stollenauskleidung mit einem weiteren hochfesten Beton.

Hydroabrasion wird massgeblich durch den Geschiebetransport verursacht, während Schwebstoffe eine untergeordnete Rolle spielen. Darum ist neben der Überwachung der hydraulischen Betriebsbedingungen das Geschiebetransport-Monitoring mittels Geophonanlage von entscheidender Bedeutung (Abbildung 5). Die Anlage befindet sich nahe des Stollenendes (Abbildung 3) und besteht aus acht Messeinheiten. Die erforderliche Kalibrierung wurde in Laborversuchen an der VAW durchgeführt und durch aufwändige Feldkalibrierungsversuche, die Bestandteil eines weiteren BFE-Forschungsprojektes (SI/500731-02) waren, erhärtet und verbessert. Damit kann der Geschiebetransport in Echtzeit überwacht und der SBT-Betrieb entsprechend gesteuert und optimiert werden.

Die Sedimentbilanz des Stausees und die Umleiteffizienz des SBTs hängen nicht nur vom Geschiebetransport, sondern auch vom Schwebstofftransport ab. Letzterer wird indirekt mittels Trübungssensoren ebenfalls simultan und in Echtzeit erfasst. Die Sensoren sind in mit Lochblechen abgedeckten Nischen in den Tunnelwänden angebracht und wurden basierend auf Schwebstoffproben kalibriert.

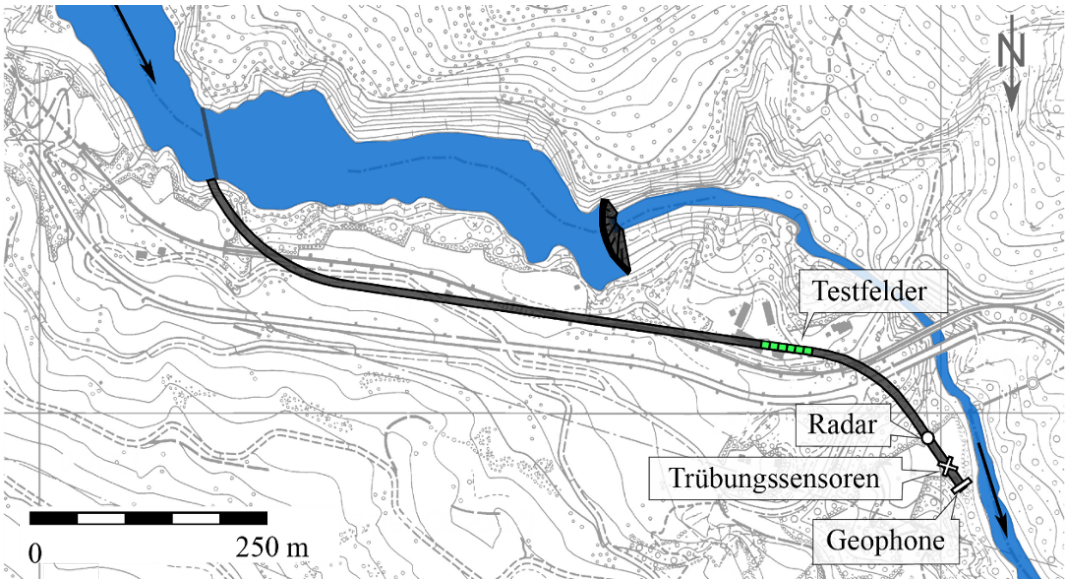

Abbildung 3: Übersicht über den Versuchsaufbau inklusive Messtechnik im SBT Solis

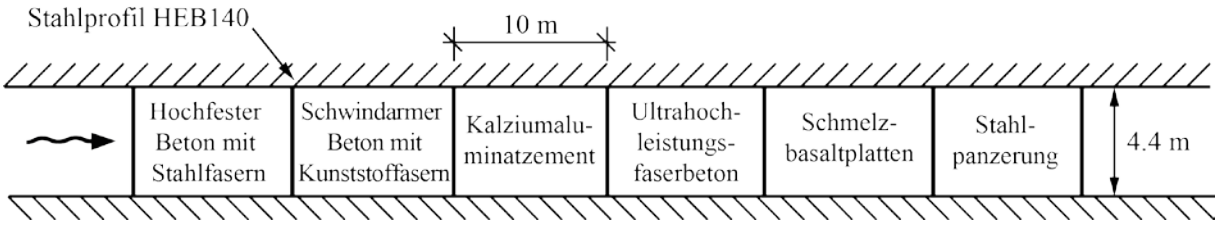

Abbildung 4: Schematische Anordnung der Testfelder im SBT Solis mit stahlfaserbewehrtem hochfestem Beton, schwindarmem Beton mit Kunststofffasern, Kalziumaluminatzementbeton, Ultrahochleistungsfaserbeton, Schmelzbasaltpflästerung und Stahlpanzerung

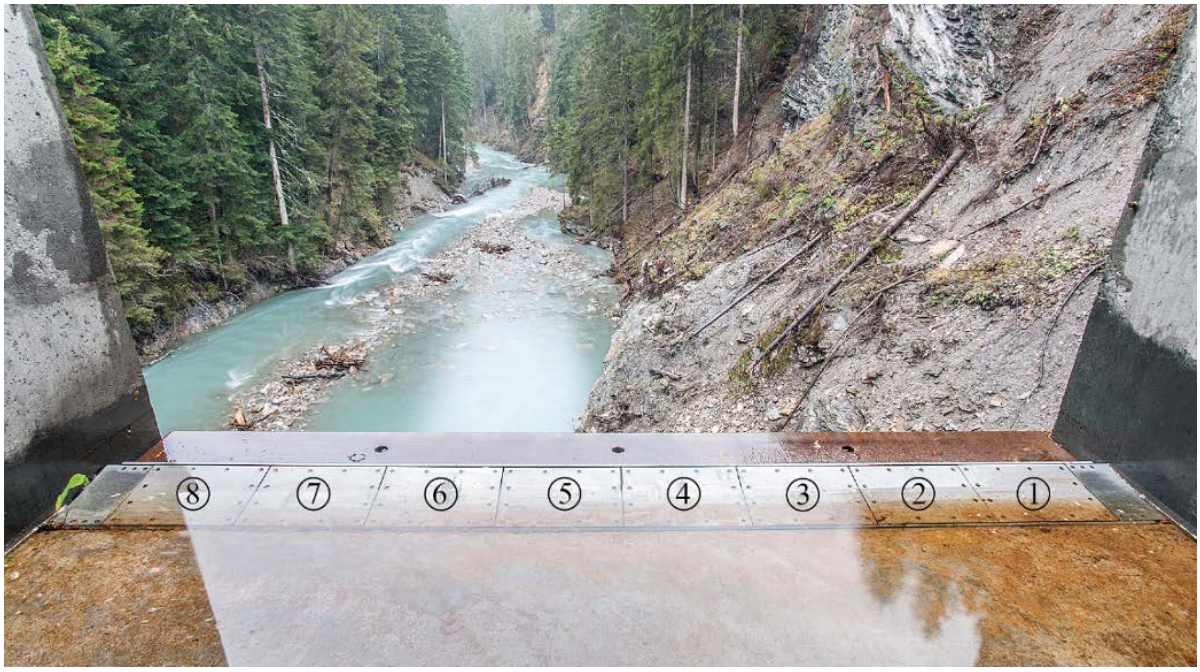

Abbildung 5: Geophonanlage am Auslauf des SBT Solis, bestehend aus acht Messeinheiten (Blick in Fliessrichtung)

Die Abrasionen wurden basierend auf 3D-Laserscanns ermittelt und als hochaufgelöste Abrasions-Topographien dargestellt. Neben mittleren Abrasionsraten soll so auch die zeitliche und örtliche Entwicklung der Abrasionsschäden bestimmt und untersucht werden. Der Initialzustand der Testfelder (sowie eines 10 m langen Abschnitts der Normsohle) wurde unmittelbar nach dem Einbau der Testfelder aufgenommen und im Zweijahresrhythmus erneut erfasst, um die Abrasionen den Einwirkungen gegenüber zu stellen.

3.2. Ökomorphologie

Die Auswirkungen des SBT-Betriebs auf die Gewässerökomorphologie der Albula wurden im 7 km langen Gewässerabschnitt zwischen dem SBT-Auslauf und der Einmündung in den Hinterrhein untersucht. Die Geometrie des Flussbetts wurde zweimal mittels LiDAR vermessen und auf morphologische Veränderungen hin untersucht. Weiter wurden die lang- und kurzfristigen Änderungen der Flussmorphologie unter verschiedenen SBT-Betriebsregimen mittels systematischen numerischen Simulationen analysiert. Die LiDAR-Aufnahmen wurden im Oktober 2014 erstmalig durchgeführt, mittels terrestrisch vermessener Flussquerschnitten validiert und im Oktober 2016 wiederholt.

4. Ergebnisse und Diskussion

4.1. Hydroabrasion

Der Versuchsaufbau wurde im Rahmen des Forschungsprojektes „Optimierung verschleissfester Materialien an Sedimentumleitstollen und wasserbaulichen Anlagen“ erstellt. Der Sedimenttransport wurde kontinuierlich mittels Geophonanlage und Trübungssensoren überwacht. Erstere dient zur

Erfassung von Sedimenten mit einem mittleren Korndurchmesser $d \geq 22$ mm (Geschiebe), letztere dient zur Detektion von Schwebstoffen mit $d < 0.5$ mm. Der Transport von Sedimenten mit einem Durchmesser von $0.5 \leq d < 22$ mm konnte messtechnisch nicht erfasst werden und wurde daher basierend auf den gemessenen Sedimentmengen abgeschätzt.

Der Stollen wurde im Frühjahr 2012 fertiggestellt und war von 2013 bis 2016 neunmal während durchschnittlich 11.9 h in Betrieb (Tabelle 1). Dabei wurden im Durchschnitt pro Betrieb $0.2 \cdot 10^3$ m^3 Geschiebe (d.h. Sediment mit $d \geq 22$ mm) und je $4.6 \cdot 10^3$ m^3 feine ($d < 0.5$ mm) und grobe Schwebstoffe ($0.5 \leq d < 22$ mm) umgeleitet. Das bedeutet, dass pro Umleitung durchschnittlich $9.4 \cdot 10^3$ m^3 an Sedimenten durch den SBT abgeleitet wurden. Dabei liegt nicht nur der Geschiebeanteil, sondern auch die Gesamtmenge an umgeleiteten Sedimenten unter den Erwartungen. Dies kann einerseits darauf zurückgeführt werden, dass sich der Verlandungskörper noch nicht in einem Gleichgewichtszustand befindet und es zu Sedimentablagerungen im Stauraum kommt. Durch Umlagerungen und Auffüllungen wird sich die Geometrie des Verlandungskörpers aber zunehmend dem Gleichgewichtszustand annähern.

Die Menge der umgeleiteten Sedimente und damit die Umleiteffizienz hängen ausserdem stark vom Betriebsregime, d.h. vom Reservoirpegel, Zufluss und Betriebsdauer ab. Dabei reagiert der Geschiebetransport deutlich sensitiver auf Schwankungen der Betriebsbedingungen als der Schwebstofftransport. Steigt der Wasserstand im Reservoir bei gleich bleibendem Zufluss über einen kritischen Wert, sinkt die Sedimenttransportkapazität im Zufluss zum SBT drastisch ab und der Geschiebetransport wird unterbunden. Die Gesamtfracht, aber auch der Geschiebeanteil, dürfte darum bei zukünftigen Spülereignissen durch die Umsetzung eines optimierten Betriebsregimes deutlich höher ausfallen.

Bathymetrische Aufnahmen der Albula in der Schinschlucht zeigen, dass sich zwischen Oktober 2014 und Oktober 2016 rund $(2.3\text{-}5.8) \cdot 10^3$ m^3 Sedimente im Unterlauf des SBTs abgelagert haben (vergleiche Kapitel 4.2).

Im gleichen Zeitraum wurden $1.1 \cdot 10^3$ m^3 Geschiebe (d.h. $d \geq 22$ mm), $21.0 \cdot 10^3$ m^3 grobe Schwebstoffe (d.h. $d = 0.5\text{-}22$ mm) und $24.5 \cdot 10^3$ m^3 feine Schwebstoffe (d.h. $d < 0.5$ mm) durch den SBT um die Sperre in die Albula umgeleitet. Unter Vernachlässigung der durch die Zuflüsse eingetragenen Sedimente und unter der Annahme, dass feine Sedimente die Schlucht ohne Ablagerung passieren, stehen die umgeleiteten Sedimentmengen in einem realistischen Verhältnis zu den Sedimentablagerungen in Unterlauf des SBTs.

Tabelle 1: Übersicht über die Betriebsereignisse des SBT Solis

SBT Betrieb	Dauer [h]	Mittlerer Abfluss [m^3/s]	Geschiebe $d \geq 22$ mm [$10^3\ m^3$]	Schwebstoffe $0.5 \leq d < 22$ mm [$10^3\ m^3$]	Schwebstoffe $d < 0.5$ mm [$10^3\ m^3$]	Totale Sedimentfracht [$10^3\ m^3$]
03. Mai 2013	16.4	68	0.02	3.1	7.0	10.1
23. Mai 2014	9.7	88	0.00	0.9	2.1	3.0
29. Juni 2014	5.3	102	0.06	1.2	2.5	3.7
13. August 2014	14.0	153	0.9	15.2	5.6	21.7
15. Mai 2015	10.7	76	0.00	1.8	4.0	5.8
09. Juni 2015	7.8	58	0.01	0.5	1.0	1.5
11. Juni 2016	13.0	80	0.2	4.2	8.4	12.8
16. Juni 2016	24.2	129	0.9	13.4	8.6	22.9
12. Juli 2016	5.5	73	0.00	1.1	2.5	3.6
Durchschnitt pro	11.9	99	0.2	4.6	4.6	9.4

Nach jedem Betrieb wurde der Stollen begutachtet und die aufgetretenen Abrasionen mittels hochaufgelöster Fotographien dokumentiert. Während im ersten Jahr keine Abrasionsspuren erkennbar waren, traten 2014 erstmals visuell feststellbare Abrasionen auf. Dabei zeigten unterschiedliche Materialien unterschiedliche Charakteristiken. Betone wiesen wellenförmige Abrasionsmuster auf, wobei die Abrasionen nach wie vor sehr gering ausfielen und von hohen Materialqualitäten zeugten. Die Zementmatrix und die Zuschläge wurden über die gesamte Fläche gleichmässig abgeschliffen, ohne dass einzelne Zementmatrixbruchstücke oder Zuschlagkörner herausgerissen worden wären (Abbildung 6a). Lokale Abrasionskonzentrationen konnten nicht festgestellt werden.

Demgegenüber wies die Schmelzbasaltpflästerung deutliche Abrasionskonzentrationen auf. Die einzelnen Platten abradierten hauptsächlich an den oberstromigen Plattenkanten (Abbildung 6b).

Die Stahlpanzerung wiederum wies zwar keinen erkennbaren flächigen Materialabtrag auf, zeigte aber deutliche Einschlagkerben (Abbildung 6c). Ausserdem wurden Unebenheiten planar abgeschliffen, so dass sich die Oberfläche unter dem Betrieb selbständig glättete. Unmittelbar nach einem SBT-Betrieb war die Oberfläche des Stahlfeldes silbrig, da sie sandstrahlähnlich poliert wurde. Anschliessend verfärbte sich die Oberfläche zunehmend. Es entwickelten sich orange bis rostbraune Muster, die den Stromlinien des anfallenden Bergwassers folgende Muster aufweisen (Abbildung 6c). Dabei verfärbten sich ständig benetzte Bereiche langsamer als wechselfeuchte Bereiche.

Der Initialzustand der Testfelder wurde von *Meisser Vermessungen AG* nach dem Einbau 2012 aufgenommen. Ende 2014 und Ende 2016 wurde der zweite und dritte Laserscan durchgeführt und die hochaufgelösten Abrasionstopographien der Testfelder erstellt (Abbildung 7). Diese deuten auf zwei unterschiedliche systematische Fehler hin. Einerseits sind kreisförmige Wellenmuster um jeden Laserstandpunkt erkennbar, andererseits ist zwischen den beiden Scanhalbkugeln ein horizontaler Versatz erkennbar. Recherchen haben ergeben, dass diese Phänomene hauptsächlich beim

eingesetzten Gerätetyp auftreten. Sie werden auf suboptimale Einsatzbedingungen (tiefe Umgebungstemperatur und hohe Luftfeuchtigkeit) sowie Staub im Innern des Gerätes zurückgeführt.

Obwohl die Schwebstofffracht die Geschiebefracht um mehrere Grössenordnungen übersteigt, spielt der Schwebstofftransport für die Abrasion im SBT Solis eine untergeordnete Rolle, da das Abrasionspotential überproportional mit der Korngrösse zunimmt. Die basierend auf den umgeleiteten Geschiebemengen berechneten Abrasionen liegen im Submillimeterbereich, was durch visuelle Begutachtungen bestätigt werden konnte. Die festgestellten Abrasionstiefen lagen damit im Bereich der Messfehler des Laserscanners und konnten weder 2014 noch 2016 messtechnisch erfasst werden. Die Abrasionsbeständigkeit der zementgebundenen Materialien wurde ausserdem in einer Geschiebetrommel untersucht (Mechtcherine *et al.* 2012). Allerdings zeigten die Ergebnisse, dass die Geschiebetrommel keine für reale SBT-Bedingungen repräsentative Resultate liefern konnte, weil die Beanspruchungsregime und Schädigungsmechanismen in der Trommel signifikant von denjenigen in SBTs abweichen. Folglich konnte die Abrasionsbeständigkeit vorerst nur qualitativ und vergleichend anhand von visuellen Begutachtungen beurteilt werden. Diese basieren auf dem Verhalten der obersten Materialschicht, welche möglicherweise nicht repräsentativ für die getesteten Materialien sind, da die Materialeigenschaften und damit das Abrasionsverhalten über die Tiefe variieren können. Um Auswertungen mit belastbaren Ergebnissen zu ermöglichen, werden darum die Versuche im SBT Solis auch nach Abschluss dieses Projekts weitergeführt.

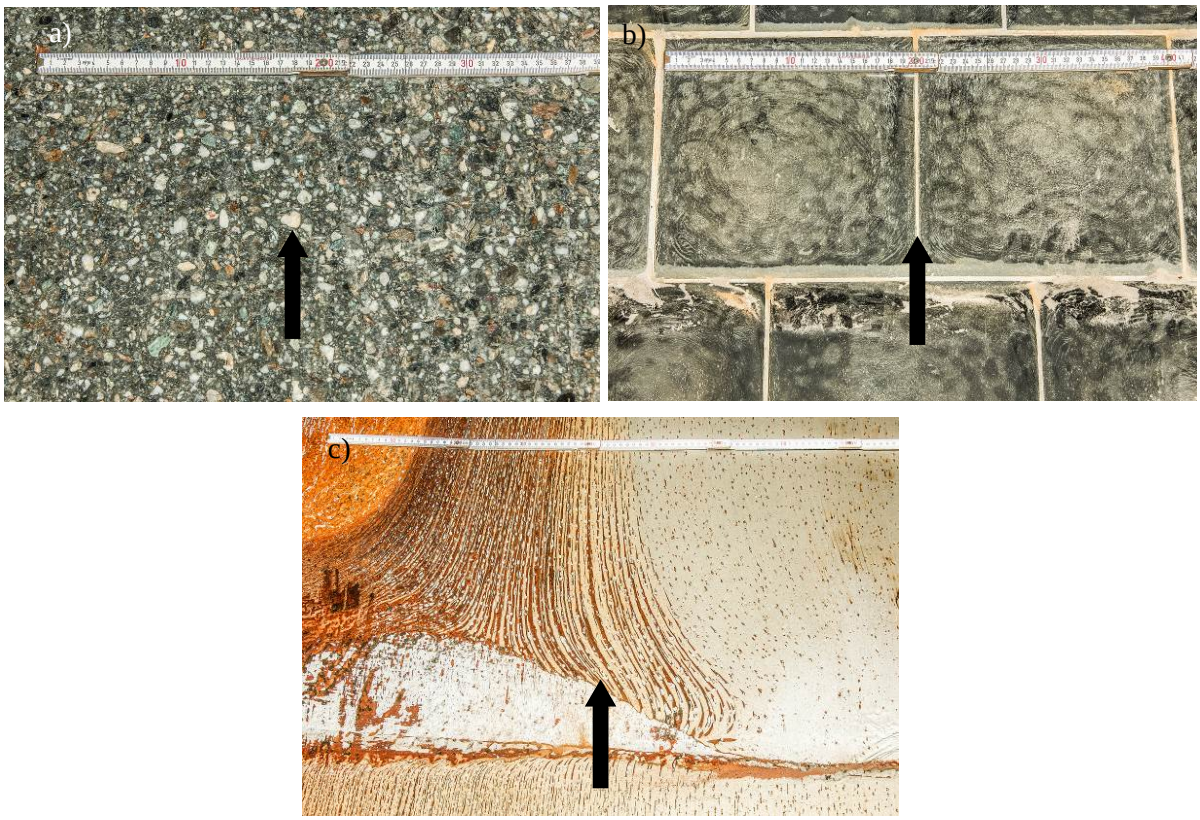

Abbildung 6: a) Abrasionen am hochfesten Betonfeld mit Stahlfasern: die Zuschläge wie auch die Zementmatrix wurden gleichermassen abgeschliffen; b) Schmelzbasaltpflästerung mit Abrasionsspuren an den oberwasserseitigen Kanten; c) Stahlpanzerung mit Einschlagskerben und planarem Abschliff von Unebenheiten; Blick immer in Fliessrichtung

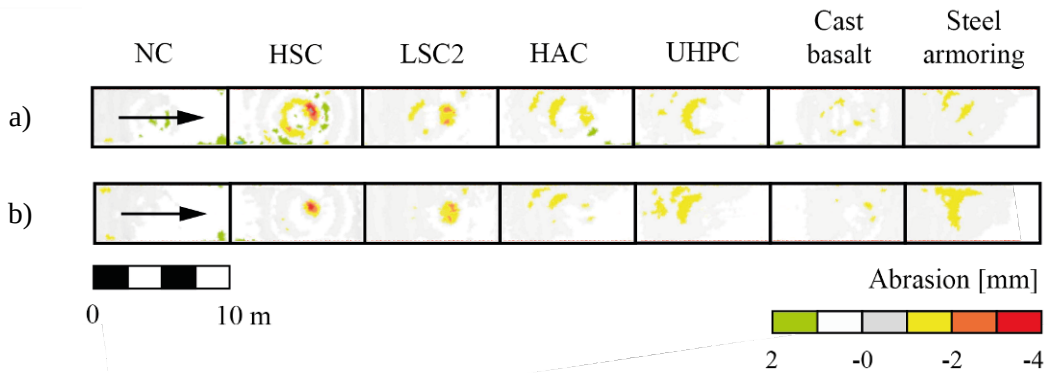

Abbildung 7: Hochaufgelöste Abrasionstopographien der Testfelder im SBT Solis, a) 2 und b) 4 Jahre nach Fertigstellung des SBT

Folgendes lässt sich für den SBT Solis zusammenfassen:

(i) Die umgeleiteten Sedimentmengen, insbesondere die umgeleiteten Geschiebemengen, lagen bisher unter den erwarteten Werten. Für beides, die insgesamt umgeleitete Sedimentmenge wie auch den Geschiebeanteil, kann in Zukunft eine signifikante Zunahme erwartet werden.

(ii) Die getesteten Materialien im SBT Solis zeigten kaum oder nur geringe Abrasionsspuren, was einerseits auf die geringen Mengen an umgeleitetem Geschiebe zurückzuführen ist, und andererseits auf hohe Abrasionsbeständigkeiten gegenüber den herrschenden Betriebsbedingungen hinweist. Die erwartete Zunahme der umgeleiteten Geschiebemengen dürfte künftig die Beanspruchung ansteigen lassen und damit zu entsprechend höheren Abrasionsraten führen. Dies soll im Rahmen eines Folgeprojektes (SI/501609-01, „Felduntersuchung von Hydraulik, Sedimenttransport und Hydroabrasion in Schweizer Sedimentumleitstollen“) untersucht werden.

4.2. Ökomorphologie

Die beiden LiDAR-Aufnahmen wurden am 18. Oktober 2014 (nach dem Ereignis vom 13. August 2014) und am 17. Oktober 2016 durchgeführt (siehe Tabelle 1). Zusätzlich wurden während der LiDAR-Aufnahmen Luftbilder gemacht (Abbildung 8). Deren Vergleich wird für die Abschätzung der flussmorphologischen Veränderungen herangezogen. Die Daten der beiden LiDAR-Aufnahmen wurden aufbereitet, d.h. es wurden Digitale Gelände Modelle (DGM) sowie Querschnittprofile erstellt (Abbildung 9). Die beiden DGM wurden zur Quantifizierung der morphologischen Auswirkungen der letzten SBT-Spülungen verglichen.

Abbildung 8: Luftaufnahme während der ersten LiDAR-Vermessung (18. Oktober 2014) von der Solis-Staumauer (links) und dem Auslaufbauwerk des Solis-SBT (rechts)

Abbildung 9: Ausschnitt des DGMs basierend auf der ersten LiDAR-Aufnahme vom 18. Oktober 2014 (Kartenquelle: Google Maps).

Die Kornverteilungsanalyse wurde in drei verschiedenen Bereichen der Schinschlucht gemacht und im Oktober 2016 abgeschlossen (Abbildung 10). Die drei gewählten Standorte sind: i) beim SBT-Auslauf (0.2 km unterhalb des SBT-Auslaufbauwerks), ii) in der Streckenmitte (2.75 km unterhalb des SBT-Auslaufbauwerks) und iii) unterhalb des letzten Zuflusses (5.5 km vom SBT-Auslaufbauwerk entfernt). Die Resultate der Kornverteilungsanalyse zeigen, dass sich die Kornverteilung des Flussbettes aufgrund der SBT-Spülung veränderte.

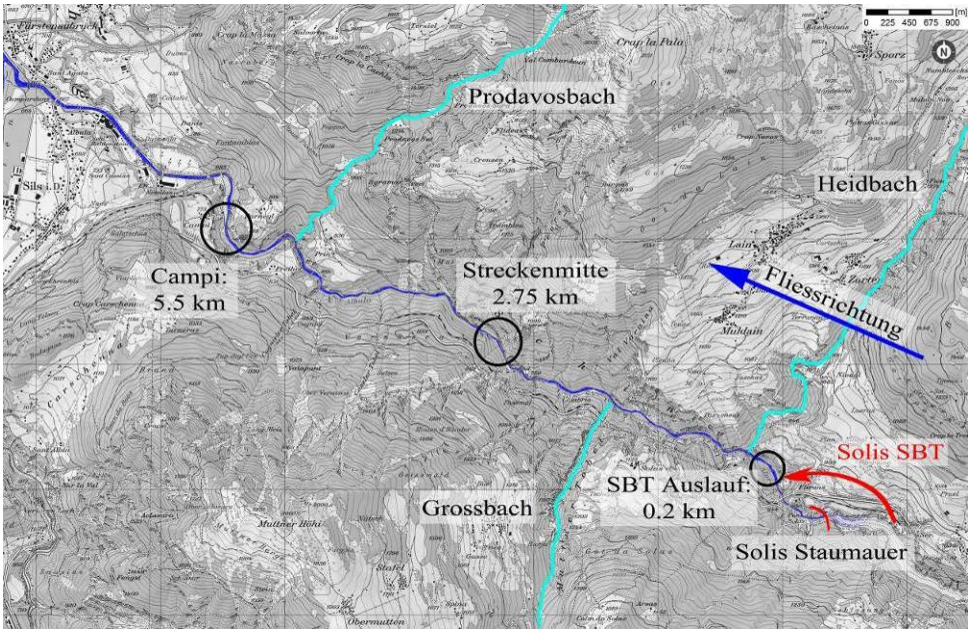

Abbildung 10: Die drei Bereiche der Sedimentproben (Kartenquelle: www.swisstopo.ch).

Mittels Vergleich der zwei LiDAR-Aufnahmen wurde die Geschiebemenge, die durch den Umleitstollen geliefert wurde, abgeschätzt. Die zwei Aufnahmen wurden während zwei Niedrigwasserperioden im Oktober 2014 und Oktober 2016 von AirborneHydroMapping GmbH (Innsbruck, Österreich) durchgeführt. Zuerst wurde die Schinschlucht mehrmals überflogen. Dann wurden die Aufnahmen abgeglichen, um eine Punktwolke zu extrapolieren. Für die beiden Aufnahmen wurde ein Laser verwendet, der mit einer Wellenlänge von 532 nm auch unter Wasserflächen messen kann, sofern die Trübung nicht zu hoch ist. Die zwei Geräte, die in 2014 bzw. 2016 gebraucht wurden, sind mit „VQ-820G“ bzw. „VQ-880G“ bezeichnet (beide Riegl Laser Measurement Systems). Der erste misst mit einer Genauigkeit von 25 mm bis zu 1 Secchi-Tiefe (z.B. Preisendorfer (1986)), der zweite mit einer Genauigkeit von 25 mm bis zu 1.5 Secchi-Tiefe. Das bedeutet, dass bei zu hoher Wassertrübung nur Aufnahmen über dem Wasserspiegel möglich sind. Die gemessene Punktdichte beträgt 20-30 pt/m2 für die Aufnahme in 2014, und 50-60 pt/m2 für die Aufnahme in 2016. Ergänzende Informationen über die zwei Aufnahmen werden in Tabelle 2 angegeben.

Tabelle 2: Übersicht der zwei LiDAR-Aufnahmen. λ_{pt} = Punktdichte am Boden, ε_{ALS} = Genauigkeit des Gerätes, ε_{geo} = Fehler bei der Georeferenzierung, ε_{str} = Fehler beim Streifenabgleich.

Jahr	Flugdatum	ALS[a] Gerät	Streifenanzahl	λ_{pt} [pt/m^2]	ε_{ALS} [cm]	ε_{geo} [cm]	ε_{str} [cm]
2014	Okt. 18	VQ820-G	16	20-30	2.5[b]	5	6
2016	Okt. 17	VQ880-G	16	50-60	2.5[c]	5	8

[a] Airborne Laser Scanning, [b] 1 Secchi-Tiefe, [c] 1.5 Secchi-Tiefe

Die Punkte der 2014er-Aufnahme wurden mittels Querschnittprofilen validiert. Die Resultate der Validierung sind in Abbildung 11 dargestellt. Die Punkte gehören zu je drei Querprofilen, die 0.2 km (SBT Auslauf in Abbildung 10) und 5.5 km (Campi in Abbildung 10) flussabwärts des SBT Solis terrestrisch im Feld gemessen wurden (rote Punkte), und von denen zusätzlich LiDAR-Daten extrapoliert wurden (blaue Punkte). Die LiDAR-Punkte stimmen mit $R^2 > 0.7$ generell gut mit den Querschnittprofilen überein.

Aufgrund der relativ hohen Wassertrübung in 2016 wurden die Punkte der 2016er-Aufnahmen mit einem neuen Verfahren validiert. Für die neue Validierung wurde zuerst mittels zweidimensionaler numerischer Modellierung die Wassertiefe geschätzt. Dafür wurde das DGM von 2014 beigezogen. Damit wurden die Punkte ermittelt, die im Tiefwasser liegen. Diese wurden dann basierend auf Intensität und Echonummer ausgewertet, d.h. Punkte, die eine hohe Intensität und eine Echonummer > 1 auswiesen, wurden als Flussbettpunkte oberhalb des Wasserspiegels bezeichnet. Die übrigen Punkte wurden dem wasserbenetzten Teil des Querprofils zugeordnet (Facchini 2017).

Nach der Validierung wurden die zwei DGM voneinander subtrahiert und das *DEM of Difference* (DoD) berechnet (Wheaton *et al.* 2010). Damit wurde das Geschiebevolumen, das zwischen Oktober 2014 und Oktober 2016 in der Schinschlucht abgelagert oder erodiert wurde, berechnet. Mit der *Geomorphic Change Detection (GCD) Software* von Wheaton *et al.* (2010) wurden die Unsicherheiten der einzelnen DGM berücksichtigt. Die einzelnen Unsicherheiten wurden ins DoD übertragen. Schliesslich wurde die Bedeutung der übertragenen Unsicherheiten bewertet.

Die Unsicherheiten der DGM können entweder als gleichverteilt im Raum oder als Funktion der Punktdichte und des Gefälles definiert werden. Dafür wurde ein *Fuzzy Inference System* (FIS) verwendet (Wheaton *et al.*, 2010) und z.B. die Resultate in Bereichen mit geringen Punktdichten und hohen lokalen Sohlgefällen als ungenau gezeichnet. Die Unsicherheiten der einzelnen DGM wurden im DoD mit folgender Formel übertragen:

$$\delta\eta_{DoD} = \sqrt{(\delta\eta_{new})^2 + (\delta\eta_{old})^2}$$

wobei $\delta\eta_{DoD}$ = übertragene Unsicherheit, $\delta\eta_{new}$ = Unsicherheit des neuesten DGM und $\delta\eta_{old}$ = Unsicherheit des ältesten DGM. Die Unsicherheit des DoD kann mit einem einfachen oder mit einem statistischen (z.B. 95%-Vertrauensintervall) Grenzwert bewertet werden. Zuletzt kann ein sogenannter *Space Contiguity Index* (SCI) verwendet werden. Dieser Index erlaubt eine räumliche Abschätzung über ausgeschnittene Zellen. Durch das SCI werden alle infolge des Grenzwertes ausgeschnittenen Zellen mit 24 Nachbarzellen bewertet. Wenn mindestens 60% der Nachbarzellen denselben Trend aufzeigen (d.h. Erosion oder Auflandung), wird die ausgeschnittene Zelle als gültig gekennzeichnet. Die Resultate und Eigenschaften der verschiedenen Analysen sind in Tabelle 3 zusammengefasst.

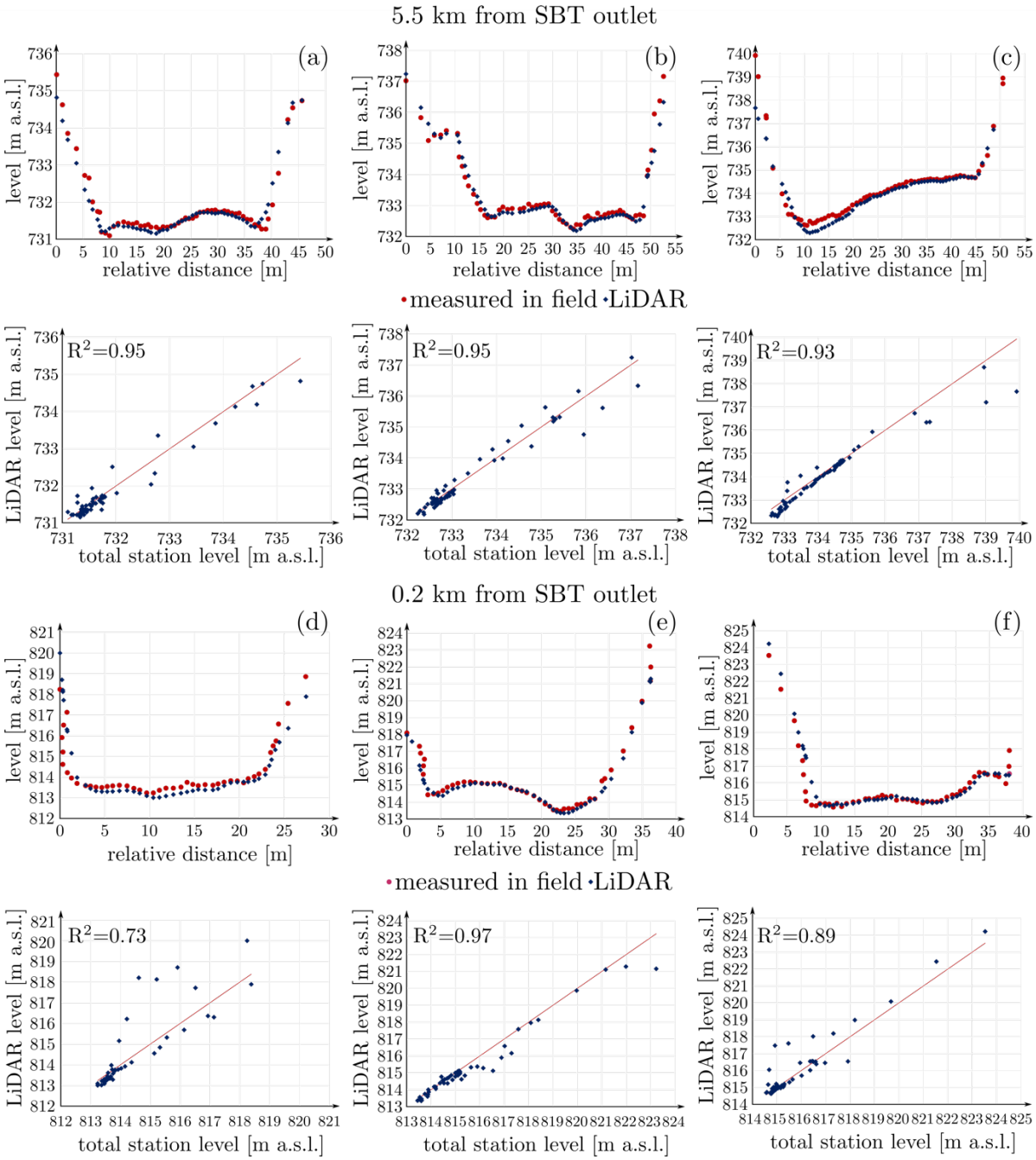

Abbildung 11: 2014 LiDAR-Validierung mit gemessenen LiDAR-Punkten (blau) und terrestrisch im Feld gemessenen Querschnittprofilen (rot).

Basierend auf den Resultaten nach Tabelle 3 überwiegen die Auflandungsprozesse in der Schinschlucht nach den SBT-Ereignissen von Juni und Juli 2016 (Tabelle 1). Das heisst, dass der Umleitstollen und die Nebenflüsse mehr Geschiebe in der Schinschlucht eintrugen, als aus der Schlucht abtransportiert wurde. Die Verteilung der Höhendifferenzen ist in Abbildung 12 dargestellt. Die Resultate zeigen, dass meisten Erosionen und Auflandungen zwischen −1.0 m und +1.0 m betragen. Unter der Annahme einer gleichverteilten Unsicherheit der einzelnen DGM werden viele kleine Höhenunterschiede vernachlässigt (z.B. Analyse 3, Abbildung 12(c)). Im Gegensatz dazu werden viele morphologische Veränderungen wiedergewonnen, wenn die DGM-Unsicherheiten als Funktion der Punktdichte und des Sohlengefälles geschätzt wurden (FIS), (z.B. Analyse 2, Abbildung 12(b)). Wenn zusätzlich das SCI angewandt wurde (Analyse 5, Abbildung 12(e)), beträgt das abgeschätzte Nettovolumen fast gleich viel wie für die grobe Analyse (basierend auf den Rohdaten, siehe Tabelle 3), weil durch das SCI nochmals zusätzliche Informationen wiedergewonnen werden.

Tabelle 3: Übersicht über die Resultate und Eigenschaften der verschiedenen DoD-Analysen. Mit V wurde das Volumen gezeichnet, mit $\delta\eta$ der Höhenunterschied.

Name	DGM Unsicherheit	DoD Unsicherheit	SCI	Erosion V [m^3]	Auflandung V [m^3]	**Netto V [m^3]**	Erosion $\delta\eta$ [m]	Aufland. $\delta\eta$ [m]
grob	keine	keine	nein	6593	12416	**5823**	0.15	0.17
1	gleichverteilt	einfach	nein	3085	5959	**2874**	0.42	0.53
2	FIS	einfach	nein	5171	10552	**5381**	0.23	0.24
3	gleichverteilt	statistisch (95%)	nein	1103	3458	**2355**	0.70	0.90
4	FIS	Statistisch (95%)	nein	3373	8138	**4765**	0.28	0.28
5	FIS	statistisch (95%)	ja	6182	11985	**5804**	0.15	0.17

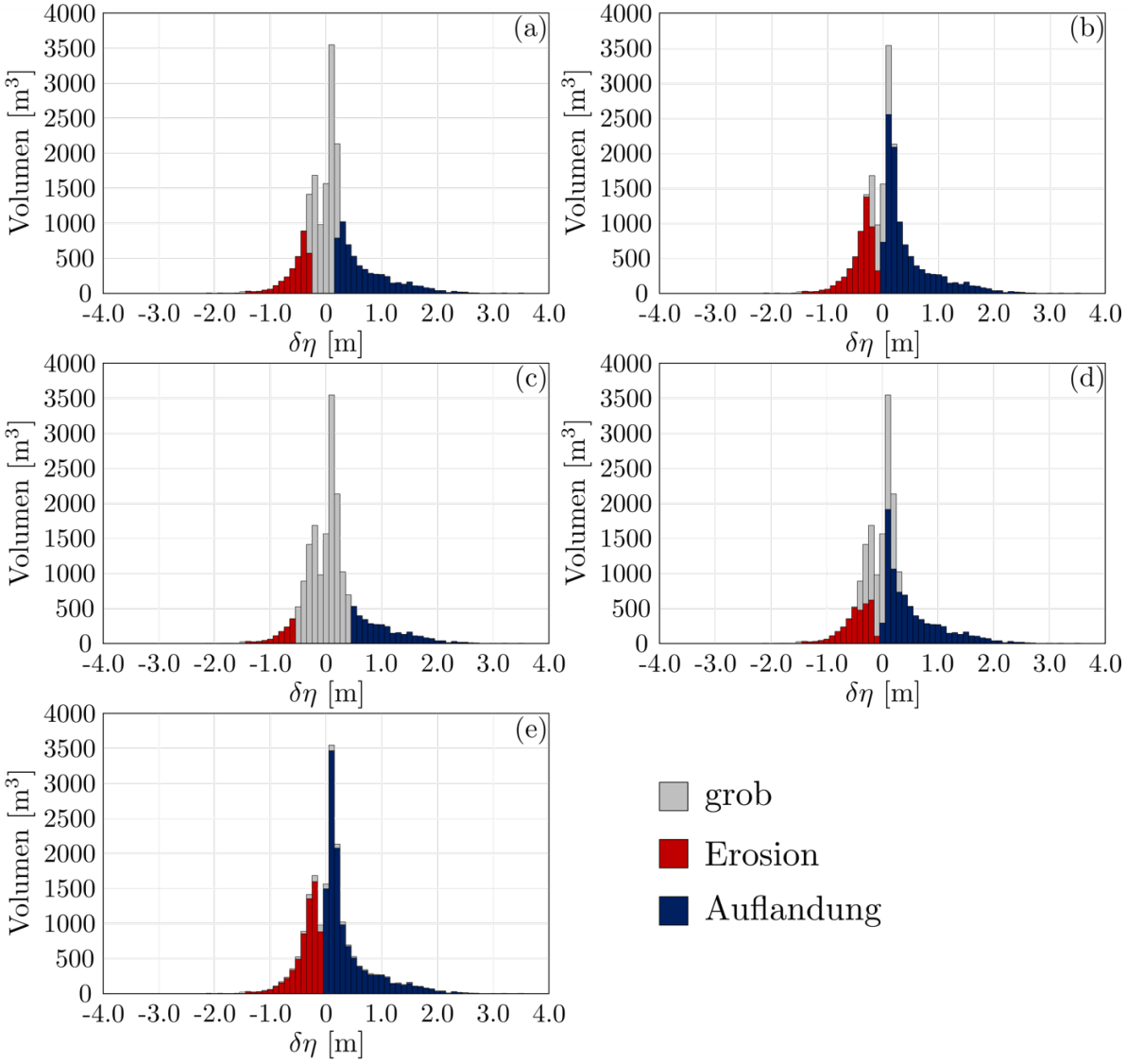

Abbildung 12: Verteilung der Höhenunterschiede unterteilt nach Erosion- und Auflandungsvolumen für die fünf verschiedenen Analysen von Tabelle 3. Erosion in rot, Auflandung in blau. Die Analyse basierend auf den Rohdaten (grob) ist grau im Hintergrund gezeichnet.

Die räumliche Verteilung der morphologischen Veränderungen für Analyse 5 ist in Abbildung 13 in Fliessrichtung dargestellt. Die Resultate zeigen, dass die Auflandungsprozesse in den ersten 2.6 km und zwischen km 3.6 und 5 konzentriert sind. Zwischen diesen beiden Bereichen wurden etwa 600 m³ erodiert. In den letzten 2 km ist die Dynamik stark von der lokalen Geometrie der Schlucht beeinflusst, weshalb ein klarer Trend schwer zu identifizieren ist. Die grösste Auflandung befindet sich direkt nach dem ersten Nebenzufluss, dem Heidbach von orographisch rechts (Abbildung 10). Die Schlucht weist dort eine Querschnittverengung und eine starke Gefälleänderung auf. Als Folge wird an dieser Stelle ein Teil des zugeführten Geschiebes abgelagert.

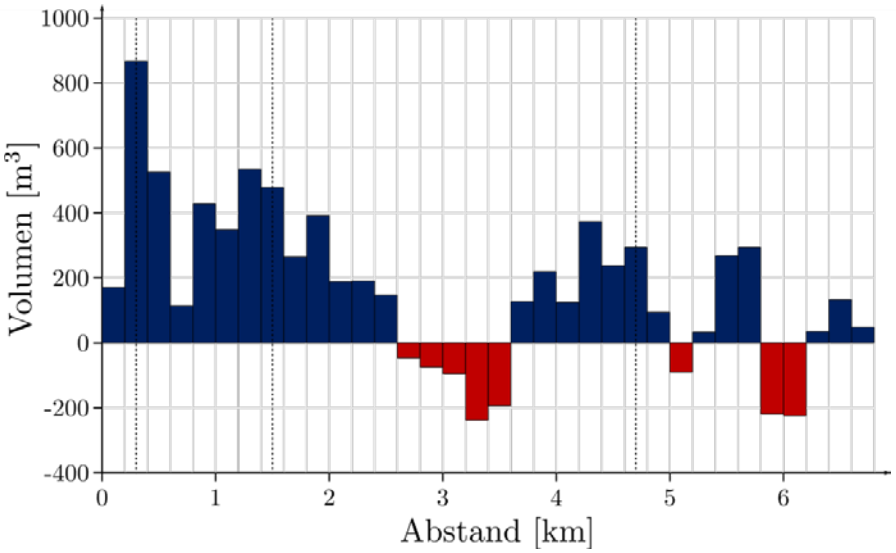

Abbildung 13: Verteilung der Auflandungs- (blau) und Erosions-Volumen (rot) in Fliessrichtung der Albula für Analyse 5 aus Tabelle 3. Die drei Nebenflüsse der Schinschlucht (siehe auch Abbildung 10) wurden mit schwarzen gestrichelten Linien dargestellt.

5. Schlussfolgerungen und Ausblick

Seit seiner Fertigstellung im Frühjahr 2012 war der SBT Solis neunmal in Betrieb. Dabei wurden im Durchschnitt $9.4 \cdot 10^3$ m³ Sedimente durchgeleitet. Dieser Wert liegt deutlich unter den Erwartungen. In Zukunft dürfte sich das Sedimentvolumen allerdings durch ein optimiertes Betriebsregime sowie die fortschreitende Annäherung des Verlandungskörpers hin zum neuen Gleichgewichtszustand zunehmen. Diese These kann im Rahmen eines Anschlussprojektes nach Abschluss des vorliegenden Projektes untersucht werden.

Die im SBT Solis eingebauten Sohlmaterialien weisen nach sechsjähriger Betriebsdauer (2012-2017, wovon im ersten und letzten Jahr kein Stollenbetrieb stattgefunden hat) nur geringe Abrasionen auf. Ein Grund dafür besteht in der relativ kleinen abgeführten Geschiebefracht und das tendenziell relativ weiche Gestein aus dem Einzugsgebiet. Weiter deuten die geringen Abrasionen auf hohe Abrasionsbeständigkeiten der eingebauten Materialien hin.

Die Abrasionsmessungen mittels 3D-Laserscanner wiesen signifikante Fehler in der Grössenordnung der aufgetretenen Abrasionen auf und liefern darum keine auswertbaren Daten. Um in Zukunft genauere Abrasionsdaten zu erhalten, werden nachfolgende Messkampagnen mit einem anderen 3D-Laser (Leica P15) durchgeführt. Die erste Aufnahme ist bereits im Frühjahr 2017 erfolgt, zeigte keine Anomalien und dient fortan als Referenz für weitere Abrasionsmessungen.

Die morphologischen Auswirkungen des SBT-Betriebs auf das Unterwasser werden von verschiedenen Variablen gesteuert. Die Menge und die Korngrössenverteilung der durch den SBT abgegebenen Sedimente, der Spitzenabfluss sowie die Form der Ganglinie aber auch die Bedingungen im Fliessgewässer vor den jeweiligen Spülungen bestimmen das Verhalten der Flussmorphologie (Facchini 2017). In der Albula unterhalb des SBT Solis sind die morphologischen Änderungen lokal, z.B.

auf Bänken, wahrnehmbar. Mittels neuester Messtechnik wurde einerseits das Volumen des durch den Umleitstollen transportierten Geschiebes abgeschätzt (Geophonanlage nach dem Prinzip des *Swiss Plate Geophone System*), andererseits die Auflandungen und Erosionen in der Albula auf 7 km Länge durch Vergleich zweier DGM bestimmt (flugzeuggestützte bathymetrische LiDAR-Messungen mit grünem Laser). Die Resultate zeigen, dass zwischen Oktober 2014 und Oktober 2016 im Saldo eine Nettoauflandung zwischen 2300 und 5800 m^3 in der Schlucht stattgefunden hat, während die Geschiebe- und Gesamtsedimentfrachten durch den SBT Solis in diesem Zeitraum bei 1100 bzw. 46‘600 m^3 lagen. Um in Zukunft genauere Ergebnisse zu erhalten, sollten die Geschiebezugaben der Nebenflüsse ebenfalls quantifiziert und berücksichtig werden.

Das vorliegende Projekt ist Bestandteil der Dissertationen von M. Facchini und M. Müller-Hagmann. Nach Abschluss der Dissertationen werden diese voraussichtlich ab April 2018 in der ETH-Bibliothek sowie als VAW-Mitteilung in elektronischer Form frei zugänglich sein:

http://e-collection.library.ethz.ch/
http://www.vaw.ethz.ch/das-institut/vaw-mitteilungen/2010-2019.html

6. Referenzen

Baumer A., Radogna R. (2015). Rehabilitation of the Palagnedra sediment bypass tunnel (2011-2013). *Proc. First International Workshop on Sediment Bypass Tunnels*, VAW-Mitteilungen 232 (R. Boes, ed.), ETH Zurich, Switzerland: 235-246.

Boes R. M., Auel C., Hagmann M., Albayrak I. (2014). Sediment bypass tunnels to mitigate reservoir sedimentation and restore sediment continuity. *Proc. International Riverflow Conference* (A. J. Schleiss *et al.*, eds.), Lausanne, Switzerland: 221-228.

Facchini A., Siviglia A., Boes R. M. (2015). Downstream morphological impact of a sediment bypass tunnel - preliminary results and forthcoming actions. *Proc. First International Workshop on Sediment Bypass Tunnels*, VAW-Mitteilungen 232 (R. Boes, ed.), VAW, ETH Zurich, Switzerland: 137-146.

Facchini M. (2017). Downstream morphological effects of Sediment Bypass Tunnels. *VAW-Mitteilungen* 243 (R. Boes, ed.), ETH Zurich, Switzerland.

Fukuda T., Yamashita K., Osada K., Fukuoka S. (2012). Study on flushing mechanism of dam reservoir sedimentation and recovery of riffle-pool in downstream reach by a flushing bypass tunnel. *Proc. International Symposium on Dams for a changing World*, Kyoto, Japan.

Fukuroi H. (2012). Damage from thyphoon talas to civil engineering structures for hydropower and the effect of the sediment bypass system at Asahi dam. *Proc. International Symposium on Dams for a changing world*, Kyoto.

Kantoush S. A., Sumi T. (2010). River morphology and sediment management strategies for sustainable reservoir in Japan and European Alps. *Annuals of Disaster Prevention Research Institute*

Kondolf G. M., Gao Y., Annandale G. W., Morris G. L., Jiang E., Zhang J., Cao Y., Carling P., Fu K., Guo Q., Hotchkiss R., Peteuli C., Sumi T., Wang H.-W., Wang Z., Wie Z., Wu B., Wu C., Yang C. T. (2014). Sustainable sediment management in reservoirs and regulated rivers: Experiences from five continents. *Earth's Future* 2 (5): 256-280. DOI: 10.1002/2013EF000184.

Martin E. J., Doering M., Robinson C. T. (2015). Ecological effects of sediment bypass tunnels. *Proc. First International Workshop on Sediment Bypass Tunnels*, VAW-Mitteilungen 232 (R. Boes, ed.), VAW, ETH Zurich, Switzerland: 147-156.

Mechtcherine V., Bellmann C., Helbig U., Horlacher H. B., Stamm J. (2012). Nachbildung der Hydroabrasionsbeanspruchung im Laborversuch Teil 1 - Experimentelle Untersuchung zu Schädigungsmechanismen im Beton ('Modeling hydroabrasive stress in the laboratory experiment, part 1 - experimental investigations of damage mechanisms in concrete'). *Bautechnik* 89 (5): 309-319 (in German).

Preisendorfer R. W. (1986). Secchi disk science: Visual optics of natural waters. *Limnology and Oceanography* 31 (5): 909-926.

Sumi T., Okano M., Takata Y. (2004). Reservoir sedimentation management with bypass tunnels in Japan. *Proc. 9th International Symposium on River Sedimentation*, Yichang: 1036-1043.

Syvitski J. P. M., Vörösmarty C. J., Kettner A. J., Green P. (2005). Impact of humans on the flux of terrestrial sediment to the global coastal ocean. *Science* 308 (5720): 376-380. DOI: 10.1126/science. 1109454.

Wheaton J. M., Brasington J., Darby S. E., Sear D. A. (2010). Accounting for uncertainty in DEMs from repeat topographic surveys: improved sediment budgets. *Earth Surface Processes and Landforms* 35 (2): 136-156.

7. Anhang

Folgendes wurde zum vorliegenden Projekt publiziert:

Facchini M., Siviglia A., Boes R. M. (2015). Downstream morphological impact of a sediment bypass tunnel - preliminary results and forthcoming actions. *Proc. First International Workshop on Sediment Bypass Tunnels*, VAW-Mitteilungen 232 (R. Boes, ed.), VAW, ETH Zurich, Switzerland: 137-146.

Facchini M., Siviglia A., Boes R. M. (2017). Downstream morphological effects of SBT releases: 1D numerical study and preliminary LiDAR data analysis. *Proc. Second International Workshop on Sediment Bypass Tunnels*, paper FP22, Kyoto University, Japan.

Hagmann M., Albayrak I., Boes R. M. (2015). Field research: Invert material resistance and sediment transport measurements. *Proc. First International Workshop on Sediment Bypass Tunnels*, VAW-Mitteilungen 232 (R. M. Boes, ed.), ETH Zurich, Switzerland: 123-136.

Mueller-Hagmann M., Albayrak I., Boes R. M. (2017). Field calibration of abrasion prediction models for concrete and granite invert linings. *Proc. Second International Workshop on Sediment Bypass Tunnels*, paper FP13, Kyoto University, Japan.

April 27-29
ETH Zurich
2015
International Workshop on
Sediment Bypass Tunnels

Downstream morphological impact of a sediment bypass tunnel – preliminary results and forthcoming actions

Matteo Facchini, Annunziato Siviglia, Robert M. Boes

Abstract

Re-establishing the sediment continuum in a river is one of the purposes of sediment bypass tunnels (SBTs). They convey sediments (bed and suspended load) from the upstream river and reservoir to the downstream reach having the potential to modify river morphology. This in turn may affect the river ecosystem altering the habitat conditions for the biota (e.g. fishes, macroinvertebrates). Understanding the effects of SBTs on river morphology is of paramount relevance for both reservoir sediment and river management purposes and is the main objective of an ongoing PhD project at the Laboratory of Hydraulics, Hydrology and Glaciology (VAW) of ETH Zurich. This project focuses on the SBT built at Solis Dam in the canton of Grisons, Switzerland, in 2012. The Solis SBT starts to effectively operate during the flood event of August 13, 2014 when about 80'000 m^3 of sediments pass through the tunnel. In this work we analyze the change in morphology that occurred during this event through a comparison between data collected in the pre-flood period (2012-2014) and those collected after the flood event. Preliminary analyses concerning cross-sectional variations and sediment grain size distributions show that changes occurred in different places downstream of the dam. Ongoing monitoring activities will provide more details on morphological changes and they serve as basis for the development of mathematical modelling aiming to predict future morphological changes and possible ecological effects, assessing different water and sediment release scenarios.

1 Introduction

Rivers are complex and dynamic systems, which are quite reactive to changes of water and/or sediment discharge regime. These changes in turn have the potential to induce dramatic morphological modifications with possible severe effects on stream ecology. The most emblematic and common anthropic cause inducing such changes is the construction of a reservoir (Graf, 2006). In most of the cases, the presence of a dam may reduce the availability of both water discharge and sediments, which in turn affect morphodynamics at a large variety of spatial scales, from the reach- to the cross-sectional scale. Rivers may change the planimetric pattern, e.g. from braided to single

thread (Surian 1999, Surian and Rinaldi 2003), or from sinuous with alternate bars to braided (Rinaldi 2003). They also can modify river cross sections in terms of bed aggradations or degradations and narrowing processes (e.g. Surian and Rinaldi 2003).

Construction of sediment bypass tunnels in dammed rivers changes the sediment discharge regime in the downstream reach, possibly inverting the morphological evolution induced by the construction of the dam (Fukuda *et al.* 2012). Effectively managing a SBT in order to both reduce the amount of sediments deposited in the reservoir and at the same time improving the ecological conditions of the downstream reach is an important task in such changing environment. In this framework, the Swiss Federal Office of Environment (FOEN) co-financed a PhD project entitled "*Re-establishment of the sediment continuum at an alpine reservoir – influence on river morphology, ecology and flood prevention*". The dammed river considered in this project is the Albula in the canton of Grisons, where a SBT has been built at Solis Dam in 2012. In August 2014, a flood with about a twenty-years return period carried approximately 80'000 m^3 of sediment through the tunnel.

The aim of this contribution is twofold. First, we present some preliminary results in which we compare different cross sections measured in the years 2012-2013 and after the 2014 flood. We also compare the sediment grain size distributions in different locations. Second, we describe field measurements and mathematical modelling activities we have planned in order to increase the knowledge about the morphological variations and the possible ecological consequences induced by SBTs.

2 Study site characteristics

The Albula River flows from the Albula pass to the Hinterrhine, draining a 950 km^2 basin. Its total length is almost 40 km. The Solis dam is located along the Albula river just downstream of Tiefencastel in the canton of Grisons (see Figure 1). It is operated by the electric power company of Zurich (ewz) and was built in 1986. It is a 61 m high arch dam with a crest length of 75 m. The catchment area at the dam amounts to 900 km^2. The Albula river reach under investigation is about 8 km long and stretches from the SBT outlet to the river mouth into the Hinterrhine (see Figure 1).

The Solis SBT was built in 2012 with a design capacity of 170 m^3/s corresponding to a five-years return period flood. The total length of the bypass tunnel is 968 m with a slope of 1.9%, except for the inflow section, which is 50 m long with a slope of 1%. The tunnel cross section has an archway shape with a width of 4.40 m and a height of 4.68 m. More details about the Solis SBT can be found in Oertli and Auel (2015).

3 The August 2014 flood

On August 13, 2014, an intense meteorological event occurred in the Albula river basin. The discharge has been measured at two gauges upstream of the SBT, on the Albula and

its major tributary, the Julia River. The gauged station located on the Albula river registered a peak discharge of 130 m^3/s (return period of about 100 years), while the gauged station on the Julia measured a peak discharge of 118 m^3/s (return period of 20 years). As a first approximation, since the two stations are close to the reservoir head and the two peaks are almost simultaneous, the two hydrographs can be summed up in order to get the inflow hydrograph ($Q_{upstream}$ in Figure 2). The peak discharge of 248 m^3/s had a return period between 20 years (HQ_{20} = 226 m^3/s) and 100 years (HQ_{100} = 282 m^3/s) (VAW 2010). During this event, water has been continuously conveyed through the SBT (Q_{SBT} in Figure 3) for about 13 hours. The total Albula discharge downstream of the bypass tunnel outlet ($Q_{downstream}$ in Figure 2) is the sum of Q_{SBT} , and both the bottom outlet discharge Q_{bo} and the spillway discharge Q_{spill} released from the dam, i.e. $Q_{downstream} = Q_{SBT} + Q_{bo} + Q_{spill}$.

Hagmann *et al.* (2015), using geophones mounted at the tunnel outlet estimated the total volume of bed load transported through the tunnel during the entire event to be about 80'000 m^3.

Figure 1: Study site: outlet of Solis SBT near Alvaschein, canton of Grisons, Switzerland (downstream view, photo by M. Facchini)

4 Morphological changes induced by the first SBT operation: Preliminary results

Field measurements have been carried out in three different locations along the 8 km river reach of the Albula River under investigations (see Figure 3): in the upper (cross sections 16-17-18), middle (cross sections 13-14-15) and downstream parts (cross sections 10-11-12) located a few hundreds of meters, 3 km and 6 km downstream of the SBT outlet, respectively. All cross sections have been measured in 2012 and 2013 and after the August 2014 flood, while the grain size distribution has been measured just in the middle and downstream parts in the same years.

The cross sections temporal evolution is given in Figures. 4a, 4b and 4c. In the upper part (Figure 4a, cross section 16) there is a trend of erosion. In the middle part (Figure 4b, cross section 13) aggradation occurred, while in the downstream part (Figure 4c, cross section 10) aggradation is evident. From these preliminary results it seems that a "sediment pulse" dynamics (Cui *et al.*, 2003, Sklar *et al.*, 2009, Venditti *et al.*, 2010, Humphries *et al.*, 2012) can be identified: once the sediments are released from the SBT, they are transported downstream as a sediment wave interacting with the pre-pulse bed material.

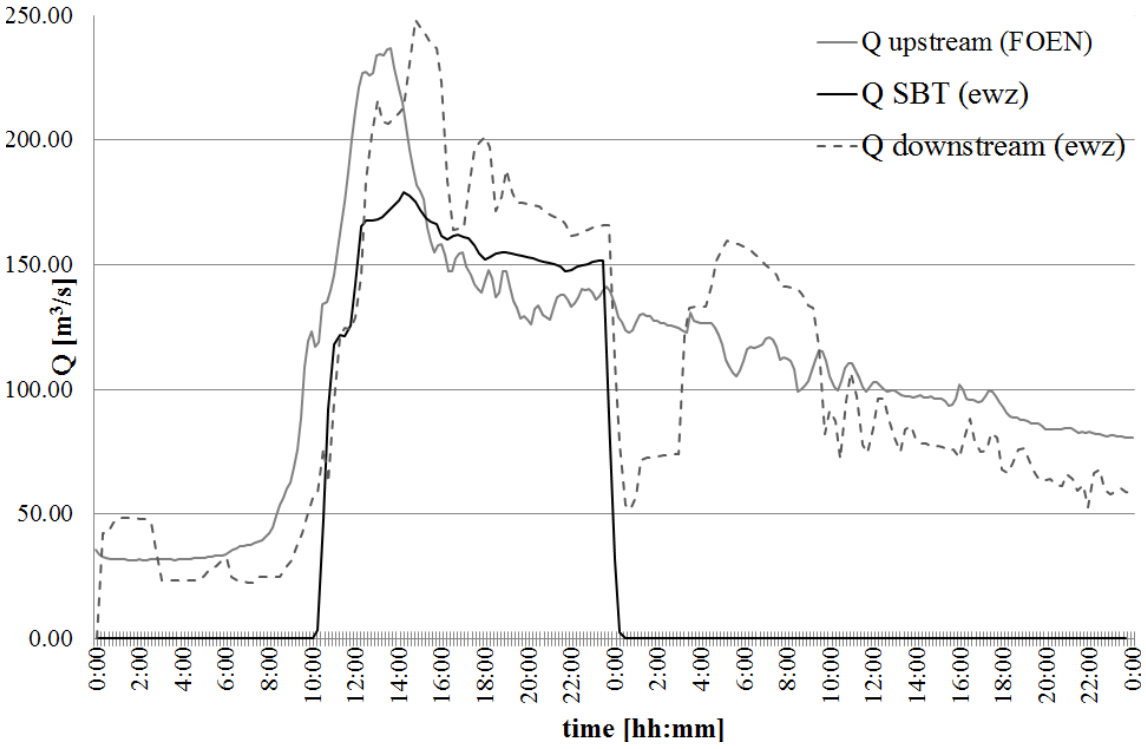

Figure 2: Hydrograph of the August 13, 2014 flood; $Q_{upstream}$ is the sum of the Albula River and Julia River discharge measured upstream of the reservoir (courtesy of FOEN), while $Q_{downstream} = Q_{SBT} + Q_{bo} + Q_{spill}$ (courtesy of ewz)

The grain size distribution is compared just in the middle and downstream areas (i.e. in cross sections 13 and 10). The results are shown in Figure 4d where we notice a coarsening trend in cross section 13 and a fining tendency in cross section 10. These results suggest that the coarse part of the sediments released by the SBT has been carried out by the flow up to the middle part of the river reach under investigation, while the finest part has been carried out for a longer distance depositing mainly in the downstream part.

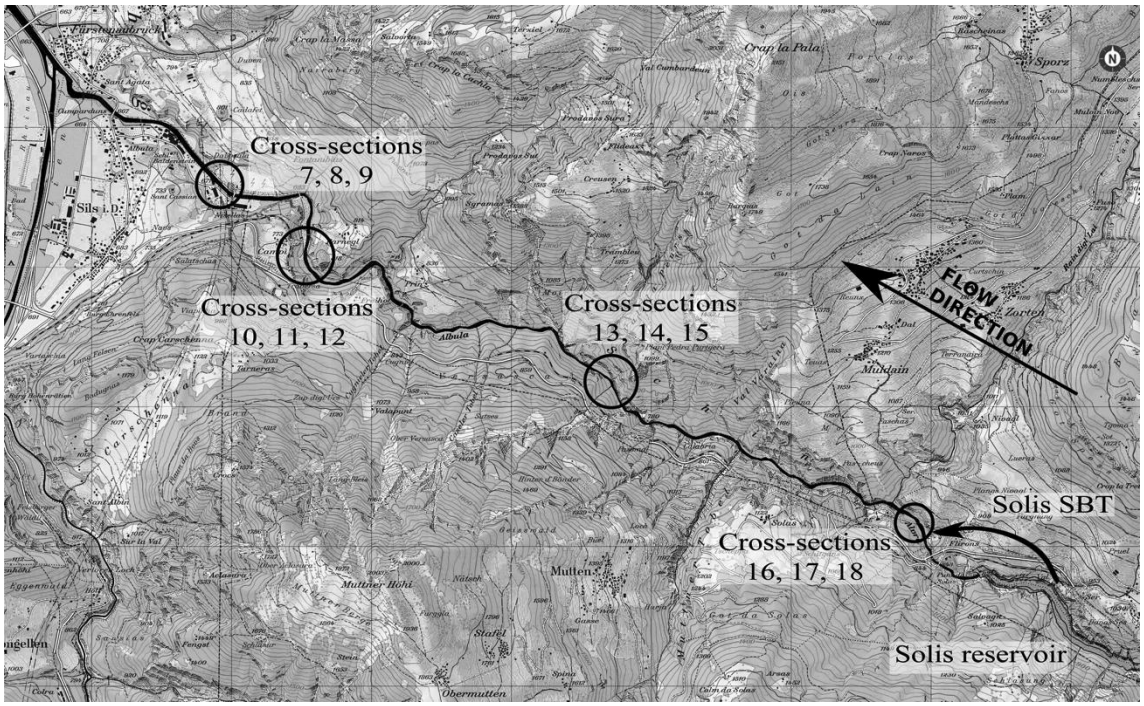

Figure 3: Cross sections measurement sites (source www.swisstopo.ch).

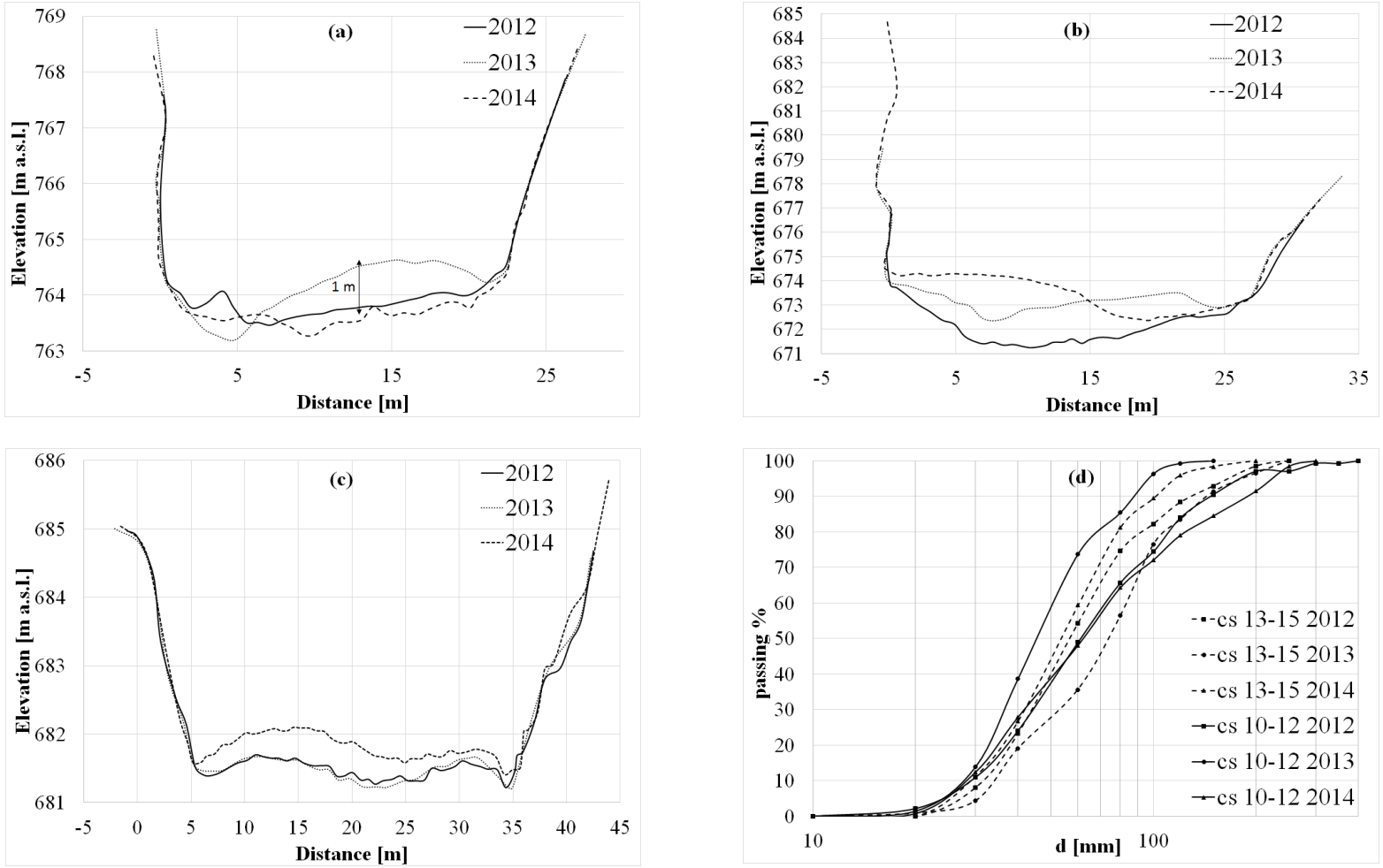

Figure 4: Cross sections 16 (a), 13 (b) and 10 (c): annual comparison (courtesy of Meisser Vermessungen AG); (d) grain size distribution comparison in 2012, 2013 and 2014 (courtesy of Hunziker, Zarn und Partner).

5 Forthcoming activities and expected outcomes

New field monitoring and mathematical modelling activities will be implemented next. Essentially the idea is to have a more detailed description of the topography in order to describe more accurately the morphological changes. These data will be used as a calibration reference for implementing mathematical modelling in order to describe future morphological changes on short (single event) and long time scale and for assessing water and sediment release management strategies. This will also allow us to use meso-habitat modelling in order to estimate the ecological consequences of morphological variations on fish habitat.

In the following we give details on single actions and tasks either planned or already in execution.

5.1 Green LiDAR survey

The green LiDAR survey is essential to have a more complete topographic representation of the river reach under investigation. A first flight has been already carried out on October 18, 2014. A second one is planned after a possible future flood, which will trigger the opening of the SBT. These data can be used for multiple purposes. First, we can analyze both the planimetric and altimetric pattern variations occurring during and between two consecutive SBT operations by comparing the Digital Elevation Models (DEM) that will be extracted from the two LIDAR flights. This allows us also to quantify the morphodynamic variations induced by the sediments introduced in the downstream reach. Second, using the aerial pictures taken during the flights we try to analyze the grain size distribution of the emerged riverbed areas with aerial photosieving: using the texture of the airborne picture we can recognize the size of the top layer particles (Dugdale *et al.* 2010) possibly identifying the grain size distribution variations.

Finally, from the LiDAR data a numerical grid will be extracted in order to run 2D numerical simulations with the software BASEMENT (Vetsch *et al.* 2014), which is able to describe morphodynamic changes in rivers. Once the morphology changes between the situations described by the two DEM will be correctly modelled, i.e. the model will be calibrated, future morphology scenarios will be numerically predicted (e.g. Brestolani *et al.* 2014) possibly including different SBT operation and reservoir management release scenarios.

5.2 Meso-habitat modification analysis

Morphological changes may in turn induce also ecosystem modifications. We will focus mainly on fish and try to quantify habitat changes adopting a reach scale approach, i.e. a meso-habitat analysis (Parasiewicz 2011, Vezza *et al.* 2014). Meso-habitats are areas inside the channel identified by different values of flow velocity, water depth and

substrate grain size. These will be measured during different field surveys to be carried out immediately afterwards the two LIDAR flights. Comparison between the two surveys allows us to quantify the meso-habitat changes induced by the SBT operations whereas two-dimensional numerical simulations will enable us to predict the evolution of the meso-habitat and to assess the effect of different release scenarios (water and sediment) on the fish habitat.

5.3 Long-term morphodynamic predictions

The aim of this task is twofold. First, from the analysis of historical airborne picture pre- and post-dam construction, we try to estimate some simple morphological evolution patterns (mainly concerning the channel width and possibly the river bed level), identifying the effect of the dam on the downstream morphology.

Second, starting from the work by Tealdi *et al.* (2011) we will try to develop a simple, lumped morphodynamic model that describes fluvial cross section dynamics consequent to changes in discharge and sediment transport induced by the SBT. The model will provide the long-term temporal dynamics of the river width and bed level. These dynamics are far from being trivial and can exhibit non-monotonic behavior, with aggradations and degradations, as well as narrowing and widening.

6 Conclusions

The analysis of the SBT operation of August 2014 shows that cross section and grain size distribution variations occurred in different places downstream of the Solis dam, along the entire river reach under investigation. Future field campaigns have been planned with the aim of accurately evaluating the morphological changes induced by SBT operations and possible ecological consequences. Finally, using numerical modelling, future release scenarios (water and sediments) will be evaluated with the aim of increasing the ecological quality of the entire river reach.

Acknowledgement

This research is supported by the *Swiss Federal Office for the Environment (FOEN)* through a PhD project embedded in the research program “Wasserbau & Ökologie”. The authors would also like to thank the companies *Hunziker, Zarn und Partner*, Domat/Ems, for the data concerning the grain size distributions, and *Meisser Vermessungen AG*, for providing us the data concerning the cross sections. We would further like to thank ewz and especially Mr. Thomas Ziegler for providing us the hydrological data concerning the dam operations.

References

Brestolani, F., Solari, L., Rinaldi, M., Lollino, G. (2014). On the Morphological Impacts of Gravel Mining: The Case of the Orco River, *Engineering Geology for Society and Territory – Volume 3(66)*, Springer International Publishing Switzerland.

Cui Y., Parker G., Lisle T. E., Gott J., Hansler-Ball M. E., Pizzuto J. E., Allmendinger N. E., Reed J. M. (2003). Sediment pulses in mountain rivers: 1. Experiments, *Water Resources Research*, 39(9): 1239.

Dugdale, S. J., Carbonneau, P. E., Campbell, D. (2010). Aerial photosieving of exposed gravel bars for the rapid calibration of airborne grain size maps, *Earth Surface Processes and Landforms*, 35(6): 627-639.

Fukuda, T., Yamashita, K., Osada, K., Fukuoka, S. (2012). Study on flushing mechanism of dam reservoir sedimentation and recovery of riffle-pool in downstream reach by a flushing bypass tunnel, *Proc. Intl. Symp. on Dams for a Changing World*, Kyoto, Japan.

Graf WL. (2006). Downstream hydrologic and geomorphic effects of large dams on American rivers, *Geomorphology*, 79(3–4, Sp. Iss. SI):336–360.

Hagmann M., Albayrak I., Boes R.M. (2015). Field research: Invert material resistance and sediment transport measurements. Proc. First Intl. Workshop on sediment bypass tunnels, *VAW-Mitteilung* 232 (R. Boes, ed.), Laboratory of Hydraulics, Hydrology and Glaciology, ETH Zurich, Switzerland.

Humphries, R.J., Venditti, J. G., Sklar, L. S., Wooster, J. K. (2012). Experimental evidence for the effect of hydrographs on sediment pulse dynamics in gravel-bedded rivers, *Water Resources Research*, 48(1): W01533.

Oertli C., Auel C. (2015). Solis sediment bypass tunnel: First operation experiences. Proc. First Intl. Workshop on sediment bypass tunnels, *VAW-Mitteilung* 232 (R. Boes, ed.), Laboratory of Hydraulics, Hydrology and Glaciology, ETH Zurich, Switzerland.

Parasiewicz, P. (2011). MesoHABSIM: A concept for application of instream flow models in river restoration planning, *Fisheries*, 26(9): 6-13.

Rinaldi M. (2003). Recent channel adjustments in alluvial rivers of Tuscany, central Italy. *Earth Surface Process Landforms*, 28(6):587–608.

Sklar, L. S., Fadde, J., Venditti, J. G., Nelson, P. A., Wydzga, M. A., Cui, Y., Dietrich, W. E. (2009). Translation and dispersion of sediment pulses in flume experiments simulating gravel augmentation below dams, *Water Resources Research*, 45(8): W08439.

Surian N. (1999). Channel changes due to river regulation: the case of the Piave River, Italy. *Earth Surface Process Landforms*, 24(12):1135–51.

Surian, N., Rinaldi, M. (2003). Morphological response to river engineering and management in alluvial channels in Italy, *Geomorphology*, 50(2003): 307-326.

Tealdi, S., Camporeale, C., Ridolfi, L. (2011). Long-term morphological river response to hydrological changes, *Advances in Water Resources*, 34(12):1643-1655.

VAW (2010). Geschiebeumleitstollen Solis - Hydraulische Modellversuche (‘Solis SBT – hydraulic model experiments‘), *Bericht* 4269, Laboratory of Hydraulics, Hydrology and Glaciology, ETH Zurich, Switzerland (unpublished).

Venditti, J. G., Dietrich, W. E., Nelson, P. A., Wydzga, M. A., Fadde, J., Sklar, L. S. (2010). Effect of sediment pulse grain size on sediment transport rates and bed mobility in gravel bed rivers, *Journal of Geophysical Research*, 115(F3): W07506.

Vetsch, D. F., Ehrbar, D. Gerber, M. Peter, S. Rousselot, P. Volz, C. Vonwiller, L. Faeh, R. Farshi, D. Mueller, R. Veprek, R. (2014). System Manuals of BASEMENT v. 2.4

Vezza, P., Parasiewicz, P., Spairani, M., Comoglio, C. (2014). Habitat modeling in high-gradient streams: the mesoscale approach and application, *Ecological applications*, 24(4): 844-861.

Authors

Matteo Facchini (corresponding Author)
Laboratory of Hydraulics, Hydrology and Glaciology (VAW), ETH Zurich
Email: facchini@vaw.baug.ethz.ch.

Dr. Annunziato Siviglia
Prof. Dr. Robert M. Boes
Laboratory of Hydraulics, Hydrology and Glaciology (VAW), ETH Zurich

May 9-12
Kyoto-Japan
2017

2nd International Workshop on
Sediment Bypass Tunnels

Downstream morphological effects of SBT releases: 1D numerical study and preliminary LiDAR data analysis

Matteo Facchini, Annunziato Siviglia and Robert M. Boes

Abstract

Sediment bypass tunnels (SBTs) are built with the twofold aim of reducing reservoir sedimentation and restoring sediment and water regimes in the downstream reach. The conveyance of water and sediment through SBTs has the potential to cause downstream morphodynamic changes, which have so far been poorly investigated. The main goal of this work is to quantify downstream morphological effects of SBT releases. This will be achieved conducting a numerical study on an idealized but still realistic situation and a field data analysis. First, assuming that the SBT transport capacity is larger than the one of the upstream river reach, we identify realistic SBT-release scenarios in terms of water and sediment discharges being released from the SBT and the dam to the downstream reach. Second, we carry out a numerical study for the quantification of the impacts of SBT operations in terms of bed level and surface sediment grain size changes. Third, we analyze the effect of the SBT releases that occurred in 2014 and 2016 at the Albula River, through a comparison of data collected during two LiDAR surveys carried out after SBT releases. Numerical results show that i) the smaller the water discharge released from the SBT, the steeper the riverbed becomes; ii) if the SBT is delivering sediment and water to the downstream reach, the riverbed grain size distribution (GSD) tends to be close to unarmored conditions, with slight changes for different release conditions. Considering a reduced SBT-efficiency (i.e. only a part of the sediment being transported in the upstream reach is entering the SBT), the described trends do not change but the equilibrium riverbed slope becomes smaller, with some release conditions causing the downstream slope to be smaller than the upstream one. Finally, from the comparison of cross-sections obtained from the points measured with two LiDAR surveys, we observe a significant depositional trend in the river reach downstream of the Solis SBT (Canton Grisons, Switzerland), as can be inferred from the numerical simulations.

Keywords: sediment bypass tunnels, gravel bed-rivers, numerical modeling, grain sorting

1 Introduction

By interrupting natural water flow and sediment regimes, dams modify river morphology with different consequences upstream and downstream of the barrage. Upstream, they confine reservoirs, thus causing the formation and development of an aggradation body

inside the reservoir, which reduces the reservoir storage capacity (Morris and Fan 1998). In the downstream reach, reduced water flow and interruption of sediment supply induce mainly channel narrowing and degradation together with coarsening of the riverbed surface (e.g. Williams and Wolman 1984). This results often in armoring of the riverbed surface, i.e. due to selective transport by size fraction the riverbed surface becomes coarser than the bedload to a great extent. Static-armoring of riverbed surfaces leads to vanishing or near-vanishing bedload transport, while mobile-armoring of riverbed surfaces allows for bedload transport of the finer fractions. If all the grain sizes present on the riverbed surface are represented in the bedload with the same fraction as on the riverbed surface, the river is in unarmored condition. That is the riverbed surface has exactly the same grain size distribution (GSD) as the bedload.

To counteract reservoir sedimentation, many techniques have been implemented at dam sites, and can be grouped in three main categories: i) sediment yield reduction, ii) sediment routing, and iii) sediment removal (Sumi *et al.* 2004). Sediment routing techniques have been proven to have positive effects in countering reservoir sedimentation (e.g. Sumi *et al.* 2004), but whether or not they can act as a mean for sediment replenishment below dam is still an open research question. On the contrary, gravel augmentation, i.e. the artificial addition of gravel to a stream, has been successfully used by hydraulic engineers, fluvial geomorphologists, and fishery biologists as a mean to mitigate sediment paucity below dams (e.g. Bunte 2004). Moreover, where sediment augmentations were difficult to perform, water releases have been used as an alternative to reactivate sediment transport and enhance habitat quality downstream of dams (e.g. Robinson *et al.* 2004).

Among the techniques used to route sediments around dams, SBTs have proven to be effective at conveying both bedload and suspended load to the downstream river reach (Sumi *et al.* 2004), but the effects of SBT releases on the downstream morphology are still poorly investigated. Moreover, the dynamic induced by sediment-laden waters released by SBTs downstream of dams is complicated by the interplay between water and sediment.

The final goal of this work is to quantify the morphological changes in terms of riverbed slope and grain size distribution (GSD) induced by realistic SBT operations. First, we identify realistic SBT-release scenarios. Second, we carry out a numerical study aiming at quantifying the morphological effects of SBT-releases. Eventually, we study the actual morphological changes occurred between two large SBT releases at the Solis dam (Canton Grisons, Switzerland) in 2014 and 2016.

2 SBT-release scenarios

Possible SBT-release scenarios are defined in terms of water and sediment discharge being conveyed through the SBT to the downstream reach. They are obtained starting

from the observation that, to properly work, a SBT must have a higher sediment transport capacity than the river flowing in the reservoir. Therefore, given the slope and the GSD of the upstream river reach, the relationship between the water Q_w and the bedload discharge Q_b (i.e. the bedload rating curve, BRC) can be calculated for the upstream (index u) river reach (BRC_u) and the SBT (BRC_{SBT}), corresponding to the solid red and blue lines in Fig. 1. We consider the SBT and dam outlets as the mean to reestablish water and sediment continuity at dams. That is, what is transported in the upstream river reach is then conveyed through the SBT and dam outlets, acting as an upstream boundary condition to the downstream river reach.

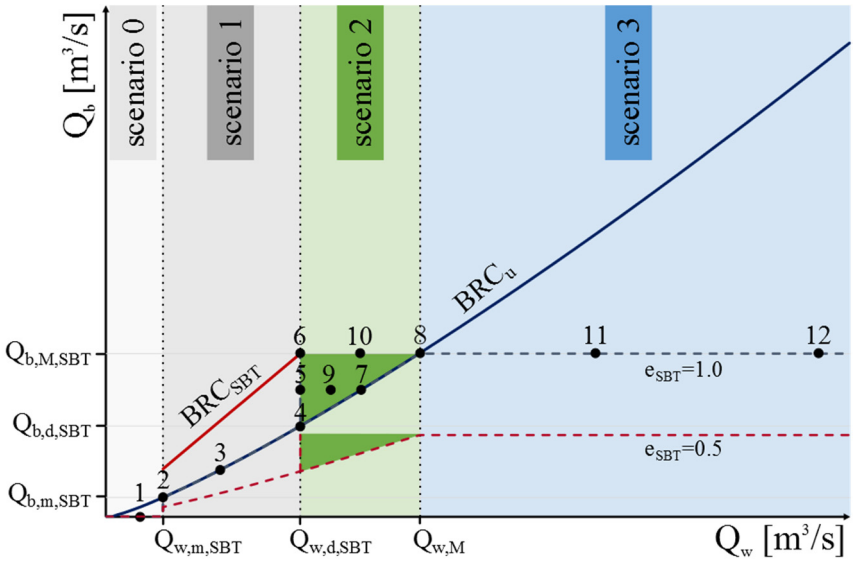

Figure 1: Bedload rating curves (BRC) for the SBT (red) and the upstream river reach flowing into the reservoir (blue); black dots and numbers refer to numerical runs; the dashed lines represent what is conveyed to the downstream reach, considering the SBT-release efficiency e_{SBT}=1.0 (grey) and e_{SBT}=0.5 (red), i.e. the SBT operating conditions.

In most of the cases, bedload and riverbed surface GSDs of rivers at which SBTs are built are composed of a mixture of sand and gravel. To take into account the effect that sand has on coarser grains, we compute the BRC_u adopting the Wilcock and Crowe (2003) sediment transport formula, while for the SBT we adopt the Smart and Jaeggi (1983) formula as suggested by Albayrak *et al.* (2016) and Boes *et al.* (2017). SBTs are usually designed (index d) according to a given water (index w) discharge value $Q_{w,d,SBT}$. On the BRC_{SBT} curve, $Q_{w,d,SBT}$ identifies the maximum (index M) bedload (index b) discharge that can be transported through the SBT ($Q_{b,M,SBT}$). The Q_w needed for carrying the maximum SBT bedload discharge in the upstream reach is termed $Q_{w,M}$. On the BRC_{SBT} curve, it is also possible to identify the minimum (index m) value of Q_w for which the SBT is first put in operation ($Q_{w,m,SBT}$), together with the corresponding minimum bedload discharge transported through the tunnel ($Q_{b,m,SBT}$). Then, we can identify four possible

scenarios in terms of water and bedload discharges released by the SBT to the downstream river reach (see Fig. 1):

- scenario 0 (very small events, i.e. $Q_w < Q_{w,m,SBT}$): the SBT is not operated and bedload carried by the upstream river, once the threshold of motion is exceeded, is all stored in the reservoir;
- scenario 1 ($Q_{w,m,SBT} \leq Q_w \leq Q_{w,d,SBT}$): the entire amount of sediment coming from upstream is diverted downstream through the SBT and the possible SBT operations are identified by the points 2, 3, and 4 lying on the BRC_u curve;
- scenario 2 ($Q_{w,d,SBT} < Q_w \leq Q_{w,M}$): the water and bedload discharges being delivered to the downstream reach range between the SBT design discharges (i.e. $Q_{w,d,SBT}$ and $Q_{b,d,SBT}$) and the maximum discharges possible (i.e. $Q_{w,M}$ and $Q_{b,M,SBT}$). This gives rise to two extreme situations: the first occurs when the water discharge fed to the downstream reach is kept constant, i.e. $Q_w = Q_{w,d,SBT}$, and the surplus, i.e. Q_w-$Q_{w,d,SBT,}$ is stored inside the reservoir, while the bedload discharge ranges between the design value and the maximum one, i.e. $Q_{b,d,SBT} \leq Q_b \leq Q_{b,M,SBT}$ (points 4, 5, and 6 in Fig. 1). The second occurs when water and bedload discharges fed to the downstream reach range both between the design and the maximum value, i.e. $Q_{w,d,SBT} < Q_w \leq Q_{w,M}$ and $Q_{b,d,SBT} < Q_b \leq Q_{b,M,SBT}$ (points 4, 7, and 8 in Fig. 1). Between these two situations a number of other release scenarios is possible, like e.g. points 9 and 10, or more generally all the points lying inside the green area bounded by points 4, 6, and 8 in Fig. 1;
- scenario 3 (very large floods, i.e. $Q_w > Q_{w,M}$): the bedload discharge fed to the downstream reach is constant and equal to the maximum transport capacity of the SBT (i.e. $Q_{b,M,SBT}$) and the water discharge increases above $Q_{w,M}$ needed to carry $Q_{b,M,SBT}$ in the upstream river reach, since extra water not flowing through the SBT is released from the dam.

The scenarios described above are obtained assuming that SBTs always work with an SBT-efficiency of $e_{SBT} = 1.0$. That is, sediment being transported in the upstream reach is conveyed entirely through the SBT. Literature studies suggest that SBTs usually do not carry all the bedload material coming from upstream, i.e. SBTs are generally characterized by $e_{SBT} < 1.0$, and it comes across that e_{SBT} decreases with increasing incoming water discharge (e.g. De Cesare *et al.* 2015). Auel *et al.* (2016) report e_{SBT}–values of 0.77 and 0.94 for the Japanese SBTs Asahi and Nunobiki, respectively, where total sediment flows are considered. For Nunobiki SBT, all coarse sediments enter the SBT even for floods with $Q_w > Q_{w,d,SBT}$ (Auel *et al.* 2016), i.e. $e_{SBT} \rightarrow 1$ regarding bedload. However, in addition to fully efficient SBTs we also consider reduced e_{SBT}–values in our runs by halving the bedload discharge Q_b being carried by the SBT, i.e. considering $e_{SBT} = 0.5$ (see dashed red line in Fig. 1).

3 Downstream morphological effects: numerical study

To quantify the downstream changes in riverbed slope and GSD due to SBT-releases, we run numerical simulations with BASEMENT (Vetsch *et al.* 2017). We consider a simplified configuration, i.e. a straight channel with rectangular cross-section 15 m wide, non-erodible walls and constant slope of 0.015. At the upstream boundary a hydrograph and a sedimentograph are imposed according to the possible SBT-release scenarios. The values relative to the hydro- and sedimentograph peaks are the ones represented by the numbered dots in Fig. 1. Water and sediment discharges vary in parallel in time and are cycled until mobile-bed equilibrium is attained. At mobile-bed equilibrium, riverbed slope and GSD are oscillating in time around defined values, due to varying water and bedload discharges at the upstream boundary. A bimodal GSD typical of a gravel bed river is fed at the upstream boundary, having 25% of sand content, geometric mean size $d_{s,g}$ = 16.22 mm and geometric standard deviation σ_g = 7.27 mm. The simplified geometry, the hydro- and the sedimentograph, and the GSD used for the numerical runs resemble the geometrical characteristics of the river reach downstream of the Solis SBT (Canton of Grisons, Switzerland), the hydro- and sedimentograph shape and duration of the August 13, 2014 flood, and the GSD of the material sampled in the vicinity of the SBT inlet structure (see e.g. Facchini *et al.* 2015).

Numerical results are given in Fig. 2 and Fig. 3, where a non-dimensional water discharge relative to the SBT design discharge, i.e. $Q^*_w = Q_w/Q_{w,d,SBT}$, is shown on the abscissa. The results on the ordinate are presented in terms of non-dimensional geometric mean size of the riverbed surface $d^*_{s,g} = d_{s,g}/d_{s,g,f}$, where $d_{s,g}$ and $d_{s,g,f}$ are the geometric mean sizes at equilibrium and of the feeding, and non-dimensional riverbed slope S^*, defined as the ratio between the final downstream equilibrium river slope S and the reference upstream slope S_{ref}, i.e. $S^* = S/S_{ref}$. The reference values we chose for $d^*_{s,g}$ and S^*, i.e. $d_{s,g,f}$ and S_{ref}, represent the target values to evaluate the effectiveness of SBT in reestablishing pre-dam conditions in the downstream reach. That is, if the goal of SBTs is reestablishing water and sediment continuity at dams, S^* = 1.0 and $d^*_{s,g}$ = 1.0 represent the situation where the downstream river reach has the same slope and riverbed surface GSD of the upstream reach. Since usually downstream reaches have lower slopes than upstream ones (e.g. Schmidt and Wilcock 2008), we can consider that $S^* > 1.0$ indicates a deposition trend, while $S^* < 1.0$ indicates an erosion trend. Moreover, the closer the riverbed surface GSD is to that of the feeding material (i.e. the closer $d^*_{s,g}$ is to 1.0), the less armored the riverbed surface (Parker and Sutherland 1990). Unarmored conditions are a favorable outcome of sediment augmentation plans below dams, since they are the opposite of what results from river damming, i.e. riverbed armoring (e.g. Williams and Wolman 1984).

Results show that final configurations have a low armoring degree of the riverbed surface, i.e. $d^*_{s,g}$ tends to 1.0 since $d_{s,g}$ tends to $d_{s,g,f}$, the higher the feeding rate. In fact, runs 6, 10, 8, 11, and 12 (connected by the dot-dashed red and blue lines in Fig. 2) have the same

equilibrium $d^*_{s,g}$, which is around 1.5 for e_{SBT} = 1.0 (blue dots in Fig. 2) and around 1.6 for e_{SBT} = 0.5 (red diamonds in Fig. 2). The riverbed GSDs at mobile-equilibrium are thus slightly different among the possible scenarios, with slightly coarser riverbeds in case of reduced e_{SBT}. Irrespective of e_{SBT}, in case of very small floods (scenario 0, run 1), the equilibrium riverbed results to be armored ($d^*_{s,g}$ > 6.0) because only water is delivered downstream, the riverbed is eroded, the transport capacity decreases and only finer grains are transported, leaving the coarser particles on the riverbed. However, the resulting GSD for run 1 is finer than the one of the static armor which corresponds to $d^*_{s,g}$ = 10.6. This is representative of the GSD obtained with the formula proposed by Parker and Sutherland (1990), which links the riverbed GSD to the transported GSD starting from the assumption that with a static armor no sediment transport takes place.

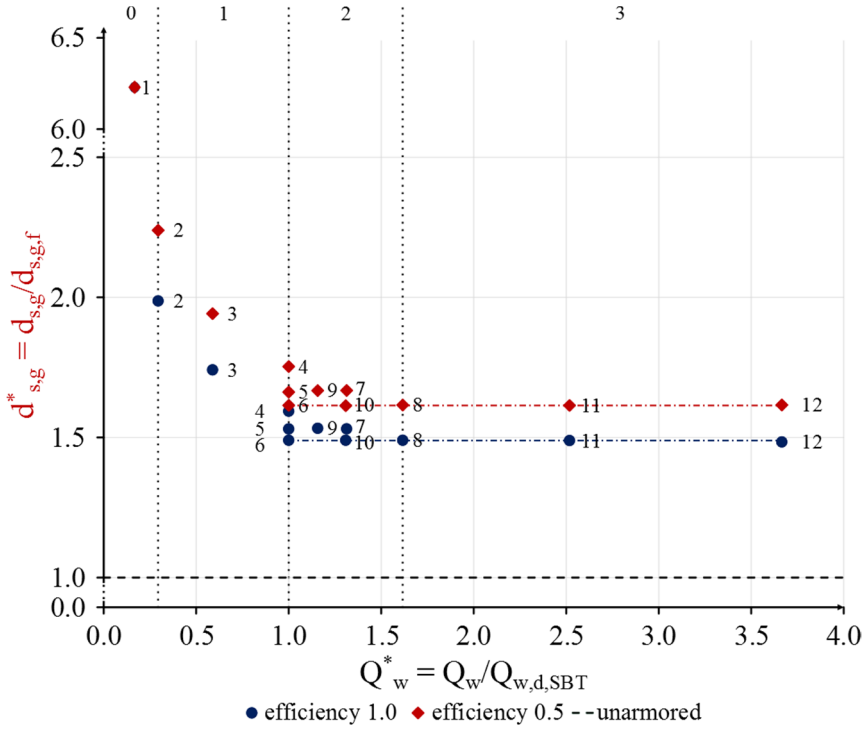

Figure 2: Results at mobile-bed equilibrium concerning bedload GSD represented by the non-dimensional geometric mean size $d^*_{s,g}$.

Concerning riverbed slopes at mobile-bed equilibrium, the results show that with e_{SBT} = 1.0, if the SBT is delivering water and sediment to the downstream reach (runs 2 to 12), they become steeper than the upstream slope, which we use as a reference (black dashed line in Fig. 3). On the contrary, assuming e_{SBT} = 0.5 results in several runs with a riverbed slope at mobile-bed equilibrium close to the upstream one (e.g. runs 3, 4, 7 and 8 in Fig. 3), and two cases (runs 11 and 12 in Fig. 3) in which the large flood water discharge results in riverbed slopes lower than the upstream one. For moderate SBT-efficiency, the downstream reach will thus be less steep than the upstream one in the case of large floods, but its riverbed surface composition will nevertheless be close to the feeding one, i.e. the

armoring degree will be far from the static armor. Regardless of e_{SBT} if the downstream reach is fed with water only (run 1), the resulting mobile-bed equilibrium slope will be considerably smaller than the upstream one.

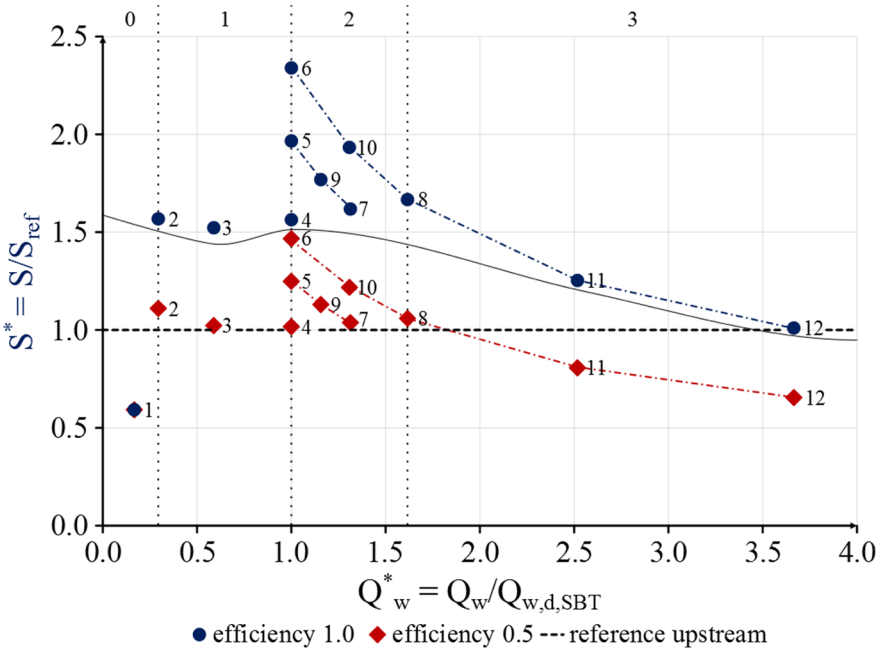

Figure 3: Results at mobile-bed equilibrium concerning riverbed slope represented by the non-dimensional slope S^*.

Another important finding is that the more water is released for a given sediment feeding rate (i.e. going from scenario 2 to scenario 3), the lower the resulting mobile-bed equilibrium slope (see the dot-dashed blue and red lines in Fig. 3), and the faster the mobile-bed equilibrium is reached. These results show that the final equilibrium configuration is dramatically dependent on the SBT-release scenario. Moreover, in the ideal case of e_{SBT} = 1.0, for each scenario in which the SBT is working (i.e. scenarios 1, 2, and 3, runs 2 to 12 in Fig. 3), the resulting riverbed slope is always higher than the upstream one.

4 Downstream morphological effects: preliminary results from field data analysis.

The Solis SBT was operated several times between 2012 (year of commissioning) and 2017, but only three operations delivered a significant amount of sediment-laden water to the downstream reach, i.e. the operation of August 13, 2014 and the two consecutive operations of June 11 and 16, 2016 (Müller-Hagmann 2017). Beside these operations, the others either delivered a negligible amount of sediment and water, or they did not last long enough to cause major changes to the downstream reach (Müller-Hagmann 2017).

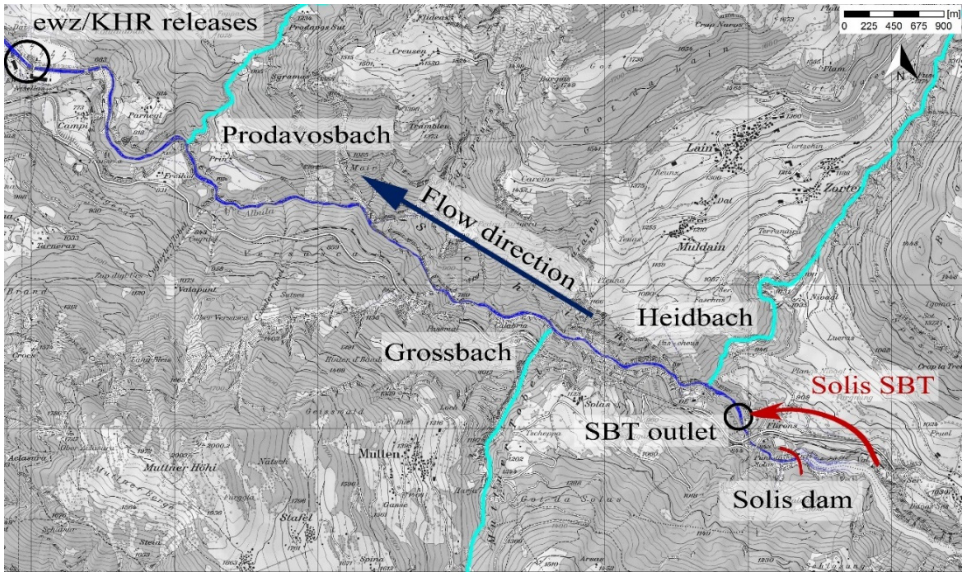

Figure 4: Plan view of Albula River between Solis dam and the intersection with the tailrace channel of the Sils hydropower plants of ewz (Elektrizitätswerk Zürich) and KHR (Kraftwerke Hinterrhein AG).

Two LiDAR surveys were performed at the Schin gorge along some 7 km downstream of the Solis dam and SBT outlet (Fig. 4) in October 2014 and October 2016, a few months after major SBT-operations. The point-clouds obtained from the LiDAR surveys have been classified to identify the measured points that are relative to buildings, vegetation, ground, and water. The identification of the water surface allows to correct the refraction-error related to the measurement of the riverbed. In fact, the performed LiDAR surveys take advantage of the use of a green laser that can penetrate the water surface and measure submerged riverbed points (e.g. Steinbacher *et al.* 2010). Then, a digital elevation model (DEM) is extrapolated from the classified point-cloud, and cross-section profiles are extracted from the DEM along the thalweg every ten meters. To estimate the changes in the cross-sectional areas, the same reference level is set below each cross-section. To minimize the error, each cross-section is cut ten meters above its lowest point (see cut level in Fig. 5), and the cross-sectional area is calculated as the area subtended from the cut cross-section (see Fig. 5).

During the operations of 2014 and 2016, the Solis SBT was operated with incoming water discharges smaller than the design discharge ($Q_{w,d,SBT}$ = 170 m^3/s, representing about a 5-year flood discharge), namely: Q_w = 153 m^3/s in 2014, and Q_w = 80 and 129 m^3/s in 2016. These values correspond to Q^*_w-values of 0.91 for 2014 and 0.48 and 0.76 for 2016. With $Q_{w,m,SBT}$ < 80 m^3/s all these releases belong to scenario 1 (see Fig. 1). We can compare the results of the numerical run with the field data analysis because the geometry used for the numerical study resembles the Albula, and the feeding GSD used for the runs is similar to the one sampled upstream of the Solis SBT. Based on the findings obtained from the numerical runs it is expected that both in the ideal case with e_{SBT} = 1.0, and in a more

realistic case with e_{SBT} = 0.5, for such values of Q^*_w, S^* is always above 1.0, i.e. $S > S_{ref}$ (Fig. 3). As the slope downstream of the Solis SBT is milder than the upstream one, we expect an increase in the downstream riverbed slope, i.e. aggradation is to be an expected outcome of 2014 and 2016 SBT releases at Solis. This is confirmed by the trend of cross-sectional area changes between 2014 and 2016 (see Fig. 6). Results presented in Fig. 6 are obtained comparing each cross-sectional area from the dataset of the two LiDAR surveys performed in October 2014 and 2016, after the 2014 and 2016 SBT operations, respectively. Since downstream of the confluence of the hydropower tailrace channel the Albula River is channelized, we plot the results relative to the first 7 km downstream of the Solis dam where the river results to be most prone to morphological changes (Fig. 4). The points relative to each cross-section are quite scattered, but the trend (dark blue solid line in Fig. 6) is clearly depositional.

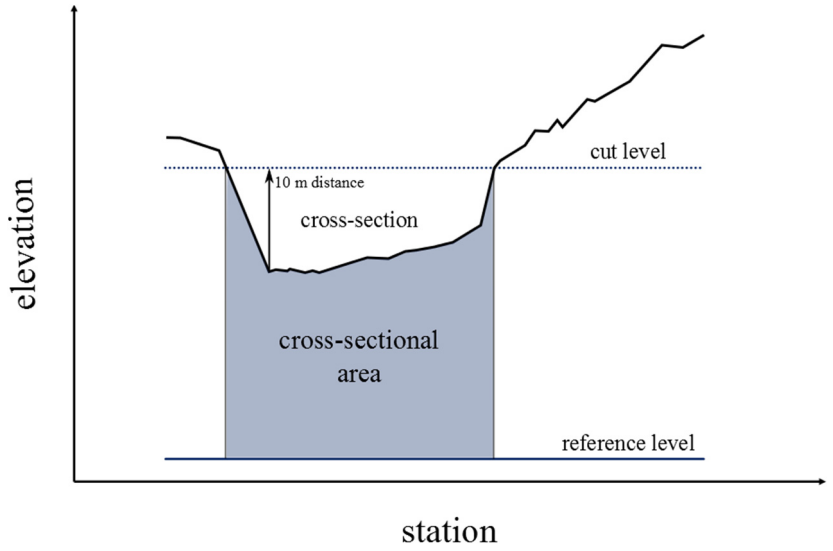

Figure 5: Sketch of a cross-section with reference level, the calculated area and the level at which each cross section is cut, i.e. ten meters above its lowest point.

5 Discussion and conclusions

A new concept for the identification of SBT-release scenarios has been developed and 1D numerical simulations have been performed to assess morphological changes caused by SBT releases. Numerical results have been verified against field data collected at the Albula River, precisely in the Schin gorge downstream of the Solis SBT. SBT-releases have the power to change riverbed slope and composition at mobile-bed equilibrium. Thereby, water and bedload discharges and bedload GSD delivered by the SBT play a major role, On the one hand, riverbed GSD approaches a static armor composition if only water is delivered from the SBT (scenario 0, $d^*_{s,g} > 6.0$). On the other hand, if an SBT is put in operation and delivers sediment-laden water to the downstream reach, the riverbed GSD approaches that of the feeding material, i.e. the riverbed becomes less armored with slight changes between different release conditions (scenarios 1, 2, and 3, $d^*_{s,g} \sim 1.5$).

Concerning riverbed slope, if no sediment is released, at mobile-bed equilibrium, the slope will be smaller than the upstream one (scenario 0, $S^* < 1$). Otherwise, at a fixed bedload feeding rate, the less water is released the steeper the riverbed becomes. While high bed slopes are a positive outcome for alpine stream morphology, since they favor the evolution of varied channel morphologies (i.e. step and pool, see e.g. Chin and Wohl 2005), an increase of the riverbed level caused by aggradation might raise the flooding danger. Eventually, halving the SBT-efficiency, i.e. the bedload discharge delivered by the SBT at a fixed water discharge, has small effects on the riverbed GSD, which becomes slightly coarser, while it has a larger impact on riverbed slope. In fact, there are several cases in which the slope is close to the upstream one (scenario 1 and some cases in scenario 2), and others in which the riverbed slope becomes smaller than the upstream one (for very large floods, i.e. scenario 3). While the SBT efficiency may thus be a mean to control riverbed aggradation if flooding becomes an issue in the downstream, a low efficiency would counteracts the reservoir desilting target of an SBT.

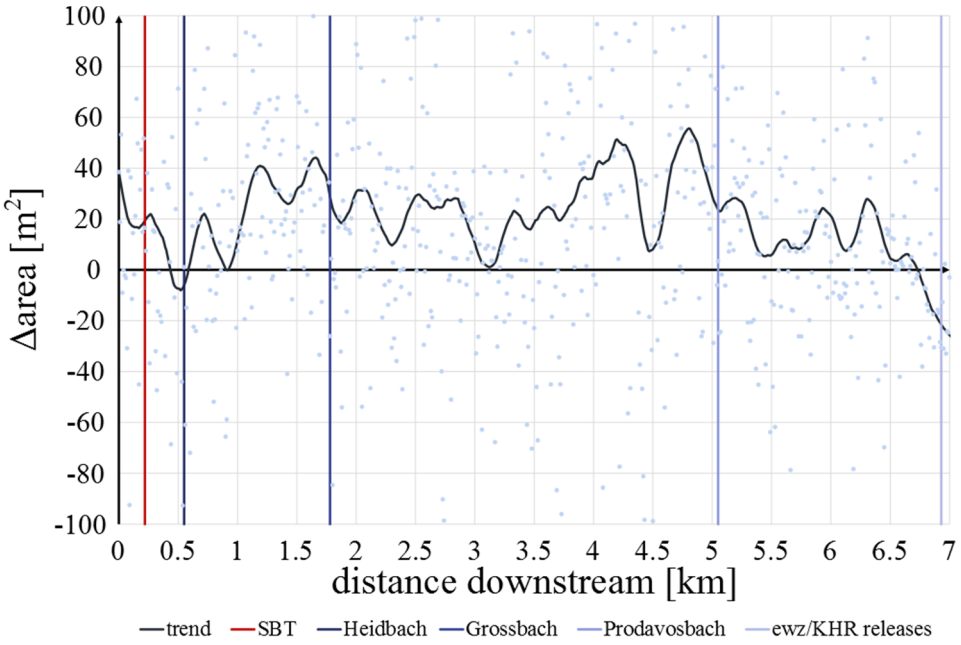

Figure 6: Cross-sectional changes between 2014 and 2016 (positive values represent deposition, negative values erosion); red vertical line represents the SBT outlet location, the other vertical lines represent major tributaries conjunctions; the dots represent single cross-sectional area changes (cross-sections are spaced along the river reach with a distance of 10 m) and the solid line represents the general trend (obtained with a zero-phase digital filtering of the scattered cross-sectional data).

Acknowledgements

The PhD project of the first author is financed by the Swiss Federal Office for the Environment (FOEN) in the “Hydraulic Engineering and Ecology” research program framework and is further affiliated to the Swiss Competence Center for Energy Research

– Supply of Electricity (SCCER-SoE). The authors would also like to thank Mr. Ziegler (ewz), Dr. Rickenmann (WSL), and Mrs. Müller-Hagmann (VAW) for providing data relative to the Solis SBT and dam operations, to the geometry of the upstream reach of the Albula River, and to water and sediment discharges in the Solis SBT, respectively.

References

Albayrak, I., Auel, C., Boes, R.M., and Müller-Hagmann, M. (2016), Mud Mountain Dam 9-foot Tunnel Re-armoring: Abrasion Calculations and Recommendations on the Invert Lining Concept, *Technical report*, Laboratory of Hydraulics, Hydrology and Glaciology (VAW), ETH, Zurich (unpublished).

Auel, C., Kantoush, S., and Sumi, T. (2016). Positive effects of reservoir sedimentation management on reservoir life - Examples from Japan. *Proc. 84th ICOLD Annual meeting* Johannesburg, South Africa**:** 4.11-14.20.

Boes, R.M., Beck, C., Lutz, N., Lais, A., and Albayrak, I. (2017). Hydraulics of water, air-water and sediment flow in downstream-controlled sediment bypass tunnels. *Proc. 2nd Intl. Workshop on Sediment Bypass Tunnels*, Kyoto, Japan.

Bunte, K. (2004). Gravel mitigation and augmentation below hydroelectric dams: a geomorphological perspective. *Report to the Stream Systems Technology Center*, USDA Forest Service, Fort Collins, USA.

Chin, A., and Wohl, E. (2005). Toward a theory for step pools in stream channels, *Progress in Physical Geography*, 29(3): 275–296

De Cesare, G., Manso, P., Daneshvari, M., and Schleiss, A.J. (2015). Laboratory research: Bed load guidance into sediment bypass tunnel inlet. *Proc. 1st Intl. Workshop on Sediment Bypass Tunnels*, Zurich, Switzerland: 169-179.

Facchini, M., Siviglia, A., and Boes, R.M. (2015). Downstream morphological impact of a sediment bypass tunnel – preliminary results and forthcoming actions. *Proc. 1st Intl. Workshop on Sediment Bypass Tunnels*, VAW-Mitteilungen 232 (R.M. Boes, ed.), ETH Zurich, Switzerland: 137-146.

Morris, G.L., and Fan, J. (1998). Reservoir Sedimentation Handbook: Design and Management of Dams, Reservoirs and Watersheds for Sustainable Use, McGraw-Hill Book Co., New York, USA.

Müller-Hagmann M. (2017). Hydroabrasion by sediment-laden high-speed flows in sediment bypass tunnels (tentative title). *VAW-Mitteilungen 239* (R. M. Boes, ed.), ETH Zurich, Switzerland: (in preparation).

Parker, G., and Sutherland, A.J. (1990). Fluvial armor. *Journal of Hydraulic Research*, 28(5): 529-544.

Robinson, C.T., Uehlinger, U., Monaghan, M.T. (2004). Stream ecosystem response to multiple experimental floods from a reservoir. *River Research and Applications*, 20(4): 359-377.

Schmidt, J.C., and Wilcock, P.R. (2008). Metrics for assessing the downstream effects of dams. W*ater Resources Research, 44(4)*: W04404.

Smart, G.M., and Jaeggi, M.N.R. (1983), Sediment Transport on Steep Slopes, *VAW-Mitteilungen 64* (D. Vischer, ed.), ETH Zurich, Switzerland.

Steinbacher, F., Pfennigbauer, M., Aufleger, M., Ullrich, A. (2010). AirborneHydroMapping – Area wide surveying of shallow water areas*. Proc. of 38th ISPRS Congres*, ISPRS.

Sumi, T., Okano, M., and Takata, Y. (2004). Reservoir sedimentation management with bypass tunnels in Japan. *Proc.9th Intl. Symposium on River Sedimentation,* Yichang, China: 1036-1043.

Vetsch, D., Siviglia, A., Ehrbar, D., Facchini, M., Kammerer, S., Koch, A., Peter, S., Vanzo, D., Vonwiller, L., Gerber, M., Volz, C., Farshi, D., Mueller, R., Rousselot, P., Veprek, R., Faeh, R. (2017). BASEMENT – Basic Simulation Environment for Computation of Environmental Flow and Natural Hazard Simulation. Version 2.7. © ETH Zurich, VAW.

Wilcock, P.R., and Crowe, J.C. (2003). Surface-based transport model for mixed-size sediment. *Journal of Hydraulic Engineering*, 129(2): 120–128.

Williams, G.P., and Wolman, M.G. (1984). Downstream effects of dams on alluvial rivers. *U.S. Geological Surveys Professional Papers*, 1286, US Geological Survey, Reston, USA.

Authors

Matteo Facchini (corresponding Author)
Annunziato Siviglia
Robert Michael Boes
Laboratory of Hydraulics, Hydrology and Glaciology, ETH Zurich, Switzerland
Email: facchini@vaw.baug.ethz.ch

April 27-29
ETH Zurich
2015
International Workshop on
Sediment Bypass Tunnels

Field research: Invert material resistance and sediment transport measurements

Michelle Hagmann, Ismail Albayrak, Robert M. Boes

Abstract

Reservoir sedimentation is a global issue affecting water supply, energy production and flood protection. For a sustainable and safe reservoir operation sediment management is mandatory. Sediment Bypass Tunnels (SBTs) are an efficient and ecological favorable measure by diverting sediment-laden inflows around reservoirs. They may prevent reservoir sedimentation and restore the downstream river reach suffering from sediment deficit. However, high flow velocities and high sediment loads cause substantial hydroabrasion wear. In the project presented herein, the abrasion resistance of different materials is investigated under field operating conditions and compared to life cycle costs by means of *in-situ* experiments. Furthermore, supplementary laboratory experiments are conducted to determine abrasion resistance of investigated materials under controlled conditions and to check and investigate upscaling from laboratory results to field applications. The abrasion resistance of materials increases with their strength. However, since hydroabrasion is a self-intensifying process starting at vulnerabilities and irregularities, implementation and curing is as important as the choice of the material itself.

1 Introduction

SBTs are an effective measure against reservoir sedimentation and contribute to a sustainable use of storage capacity for water supply, energy production and flood control. They divert sediment-laden inflows around dams and thus may restore the natural sediment continuity that is disturbed by dam construction. Due to climate change and population growth sustainable sediment management at reservoirs gained increasing importance and SBTs have recently attracted growing attention, especially in mountainous regions in Asia and South America. However, SBTs are subjected to strong abrasion due to high flow velocities and sediment transport rates causing high annual maintenance expenses in the range of 1% of the investment costs (Auel 2014). An impressive example showing massive damages is the Palagnedra SBT in southern Switzerland (Vischer *et al.* 1997). After a flood event in 1978 the corresponding hydropower plant was shut down and the Melazza River was diverted through the SBT during the refurbishment period of 10 months (Delley 1988). The concrete invert was destroyed and the incision channel depth reached up to 2.7 m into the bedrock (Figure

1). In order to enhance the cost-effectiveness of SBTs suitable invert materials are indispensable.

Therefore a research project was initiated at the Laboratory of Hydraulics, Hydrology and Glaciology (VAW) of ETH Zurich (Hagmann *et al.* 2012, Boes *et al.* 2014, Hagmann *et al.* 2014). The main objectives are to quantify the correlations between the hydraulic operation conditions, sediment load, invert material properties and measured hydroabrasion. To achieve this goal, *in-situ* experiments in Solis, Pfaffensprung and Runcahez SBTs are conducted.

Figure 1: Invert damages at the Palagnedra SBT (Canton Ticino, Switzerland) after an exceptional flood event in 1978 (IM Maggia Engineering AG)

Furthermore, the transferability of laboratory results to field scale is investigated in collaboration with the Institute of Construction Materials of TU Dresden, Germany. Therefore specimens of invert materials from Solis and Pfaffensprung SBTs have been tested in the laboratory and compared to their *in-situ* performance (Bellmann and Mechtcherine 2012, Mechtcherine *et al.* 2012). Finally, outputs of this project together with results of a precedent study on sediment transport and abrasion processes in SBTs (Auel 2014) will help operators of hydraulic systems facing abrasion problems by giving recommendations of SBT design, economical invert materials and their implementation. Herein, the experimental setups, the sediment transport monitoring system, and the recently obtained results are presented.

2 Instrumentation

2.1 Monitoring of hydraulic conditions

To adequately estimate the discharge in the tunnel, precise knowledge of the flow velocity and flow depth is needed. Pressure sensors are popular, competitive and robust devices for the determination of water depth under subcritical flow conditions. However, under the supercritical flow conditions prevailing in SBT, it is difficult to soundly mount these devices in tunnels without disturbing the measurements.

Another commonly used method for continuous and real-time monitoring of hydraulic operating conditions is the radar technique. This is a contact-free technique applicable also under supercritical flow conditions. It determines water levels by measuring time between sent and received pulses. Furthermore, it also measures surface flow velocity using the Doppler Effect. Finally, the discharge is determined based on the continuity equation and a site specific conversion factor adapted from water depth, cross section and surface flow velocity.

2.2 Sediment monitoring

Sediment load is divided into bed load and suspended load. For bedload monitoring there are various techniques available (Bogen and Møen 2001, Gottesfeld and Tunnicliffe 2003, Rickenmann and McArdell 2007, Møen *et al.* 2010). For the present research project, a robust, accurate and continuous real-time measurement technique is needed to monitor sediment load in SBTs. The Swiss plate geophone developed at the Swiss Federal Institute for Forest, Snow and Landscape Research (WSL) fulfills these requirements (Rickenmann and McArdell 2007, Rickenmann *et al.* 2012, Wyss *et al.* 2014). The device consist of an elastically bedded (elastic polymer type "CR/SBR Standard 65±5", manufactured by Angst + Pfister, Zurich, Switzerland) steel plate (S235; l=492 mm, w=358 mm, t=15 mm) mounted by a steel profile (S235, UPE400) flush to the channel invert (Figure 3). Bedload particles impinging the plate cause oscillations which are registered by a geophone sensor (Geospace GS-20DX, manufactured by Geospace Technologies, Houston, Texas) attached on the rear side of the plate within a waterproof casing. The sampling rate is 10 kHz and thus allows sampling of the plate oscillations.

When the signal voltage exceeds a certain threshold value corresponding to vibrations due to clear water background noise, an impulse is registered. The number of impulses correlates linearly with the sediment transport rate whereas the grain size distribution can be estimated based on the maximal amplitude value (Rickenmann *et al.* 2012, Wyss *et al.* 2014). However, correlation between registered signals and sediment transport rate, is strongly site-dependent. Hydraulic flow conditions, particle size distribution and particle shape affect the measurement signal. Therefore a calibration, in best case *in-situ*, is required for every single geophone system. Under controlled laboratory

conditions (mean flow velocity of 4 m/s, water depth of 10 cm) the threshold for detected grain was determined being between 2 and 3 cm for the horizontal arrangement of a geophone system. Furthermore, threshold grain size was significantly lowered by inclining the geophone 10° against the channel bottom slope (Morach 2011).

Turbidimeters are a popular and commonly used optical device for suspended sediment measurements at rivers, lakes, desilting basins and power plants (Grasso *et al.* 2005, Habersack *et al.* 2008). The devices register either the backscatter or the transmission of the emitted visible or infrared light. The signal output is turbidity and has to be converted to suspended sediment concentration using a calibration curve. Therefore, bottle samples are taken regularly from the river. Their calibration is affected by particle shape, size and color (Felix *et al.* 2013). Depending on particle properties the measurement range varies from several milligram per liter up to hundred grams per liter (Black and Rosenberg 1994, Wren *et al.* 2000).

2.3 Abrasion measurement

Abrasion can be measured either by hand using a leveling rule or by use of 3D-laser-technique. Jacobs *et al.* (2001) used the former to measure the abrasion in the Runcahez SBT. Also the abrasion at Asahi SBT, Japan and the abrasion in the Runcahez SBT is measured similarly (Jacobs and Hagmann 2015, Nakajima *et al.* 2015).

However, the advantage of a 3D-laser technique is the provision of high resolution surface maps. Furthermore the measurement process is much less time consuming compared to the leveling rule method. Maps obtained at different stages are used to evaluate temporal and spatial development of abrasion occurring on the surface. Depending on the specifications, 3D–lasers are applicable up to 100 m distance measurements with measurement errors around ± 2 mm. In order to obtain a surface map with high resolution and minimal errors around ± 1 mm, the measurements distance is kept in the range of 1.5 to 10 m.

3 Experimental setups and methodology

3.1 Solis SBT

The Solis SBT located in the Swiss Alps was commissioned in 2012 (Oertli 2009, Auel *et al.* 2011, Oertli and Auel 2015). The SBT intake is located 804.5 m asl. For SBT operation the reservoir level partially lowered (active storage volume: 823.75 and 816 m asl, target SBT operation level: 816 and 814.5 m asl) resulting in pressurized flow conditions at the intake. After the intake flow conditions change to supercritical free surface flow with flow velocities up to 11 m/s.

The SBT houses six test fields, each 10 m long, with different abrasion-resistant materials. Four concretes with different compressive strengths and mixtures, cast basalt tiles and steel plates were implemented directly upstream of the right bend (Hagmann *et*

al. 2012) (Figure 2). In combination with the high-performance concrete invert of Solis SBT, a total of seven different invert materials are tested. For separation of the single trial fields and for proper implementation, steel beams were installed at the end of every field.

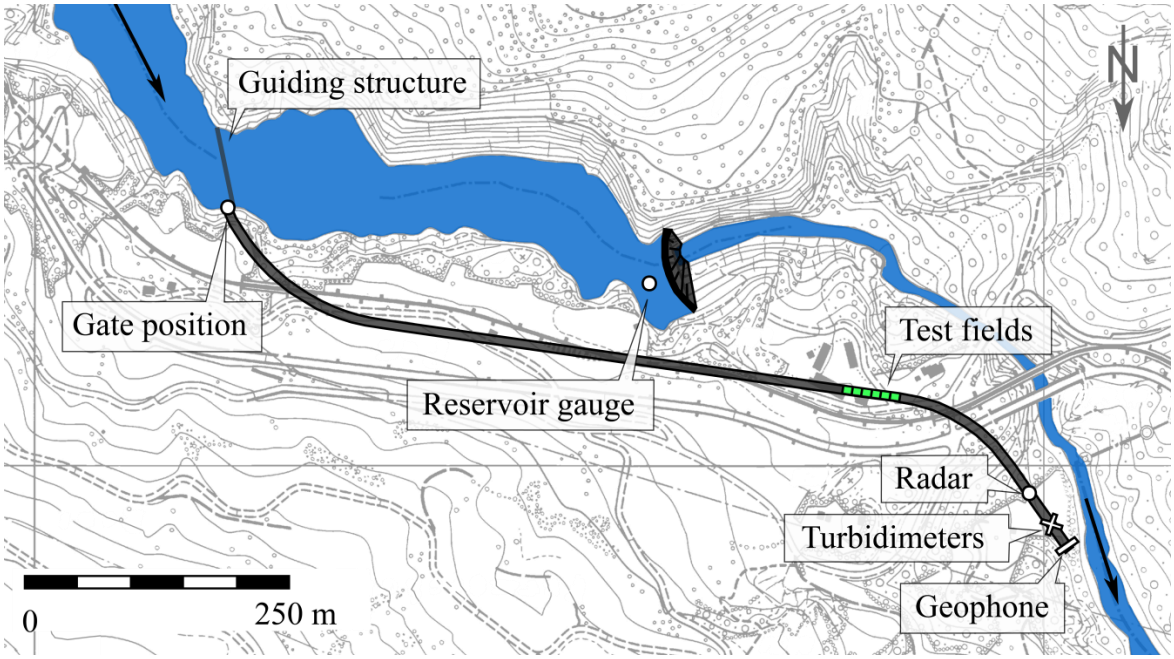

Figure 2: Overview of the Solis SBT with test fields and the instrumentation

Hydraulic conditions in the tunnel and reservoir are monitored using a radar system mounted on the tunnel ceiling (RQ-30, manufactured by Sommer Messtechnik, Koblach, Austria), two pressure sensors installed at both tunnel walls (Probe 26 W, manufactured by Keller AG, Winterthur, Switzerland), and a pressure transmitter measuring the reservoir level (MPA, manufactured by Rittmeyer, Baar, Switzerland), respectively. Furthermore, the position of the intake gate is observed by displacement transducers.

Both, the gate position and the reservoir water level are used in combination with hydraulic model test results (Auel *et al.* 2011) to estimate the discharge. These results can be compared to the measurements using the radar and pressure sensors in the tunnel. The sediment transport is monitored by two turbidimeters installed next to the pressure sensors in the side wall recesses (TubiMax W CUS41, manufactured by Endress+Hauser, Reinach, Switzerland) and by an in-house-constructed geophone system consisting of eight units at the SBT outlet (Figure 3). Generally, the sampling rate is 1/60 Hz, except for the geophones, where it is 10 kHz. The data acquisition is triggered by the SBT intake gate opening.

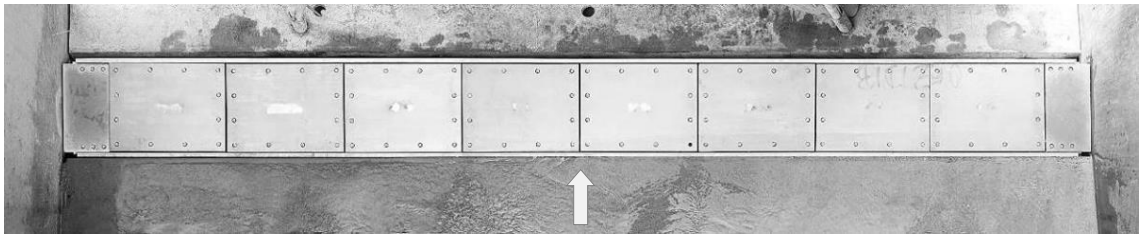

Figure 3: Picture of the geophone system consisting of eight units across the tunnel width, installed at the outlet of Solis SBT; flow direction from bottom to top

The surface of the tunnel invert is mapped by a laser scanner (FARO Focus 3D, manufactured by FARO, Lake Mary, United States). The first measurement was performed in 2012 after implementation. After every significant event provoking invert abrasion further scans are conducted.

3.2 Pfaffensprung SBT

The Pfaffensprung SBT located in the Swiss Alps was commissioned 1922 together with the Pfaffensprung reservoir erected for hydropower generation (SBZ 1943, Vischer *et al.* 1997, Müller 2015). The tunnel is in operation for over 100 days per year when the inflow exceeds the threshold discharge for bedload transport. The operating flow velocities lay between 15 and 17 m/s.

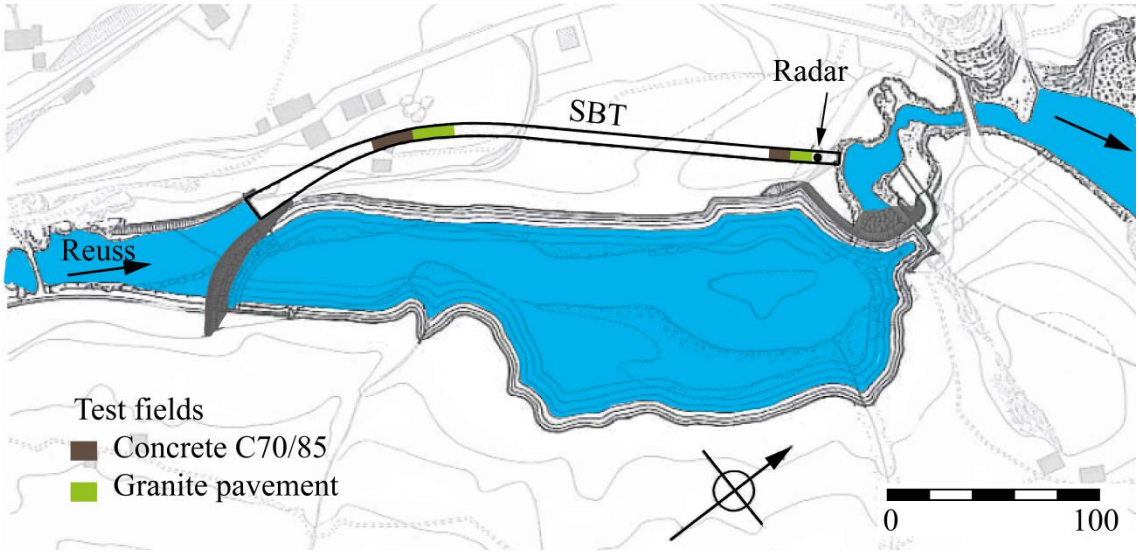

Figure 4: Overview of the Solis SBT with location of test fields and instrumentation

In the winter season 2011/12 and 2012/13 10 m long tests fields were implemented near the outlet and in the tunnel bend (Figure 4). They consist of a granite pavement and high-strength concrete with and without steel fibers. The original layer thickness was 30 cm. Compression strengths of granite and concretes are f_c = 180 MPa, 75 and 79 MPa, respectively. The hydraulic operating conditions are monitored by a radar mounted on the ceiling near the outlet (Vegaplus 54K, manufactured by Vega,

Pfäffikon, Switzerland) while the invert abrasion is determined based on measurements taken every winter season by a 3D-laser scanner (Z+F Imager 5006h, manufactured by Zoller + Fröhlich, Wangen im Allgäu, Germany).

3.3 Laboratory tests

To simulate hydroabrasion in the laboratory at controllable conditions a rotating drum developed at the Technical University of Dresden is used (Bellmann 2012, Mechtcherine *et al.* 2012). It consists of an octagonal rotating drum, feed with an abrasive charge and equipped with slab shaped specimens (300 mm × 300 mm × 50 mm). By changing abrasive particle size and rotation velocity, different flow and sediment load regimes are simulated (Bellmann 2012, Mechtcherine *et al.* 2012). The abrasion is determined both by weighing and laser scans providing the parameters abrasion rate, mass loss, and abrasion depth, respectively.

4 Results

4.1 Solis SBT

Since the commissioning, the Solis SBT was in operation four times. It was found that the sediment transport rate changed as a function of the reservoir level, corresponding to an increasing energy head, and suspended sediment rate scattered larger than bed load (Figure 5a and Figure 5b). With increasing reservoir level the bed shear stress upstream of the intake decreases due to the low flow velocity, and reduces the sediment transport capacity leading to lower sediment transport rates in the reservoir and thus in bypass tunnel itself. Reasons for the fluctuations are assumed to be generated by local erosions of the aggradation body.

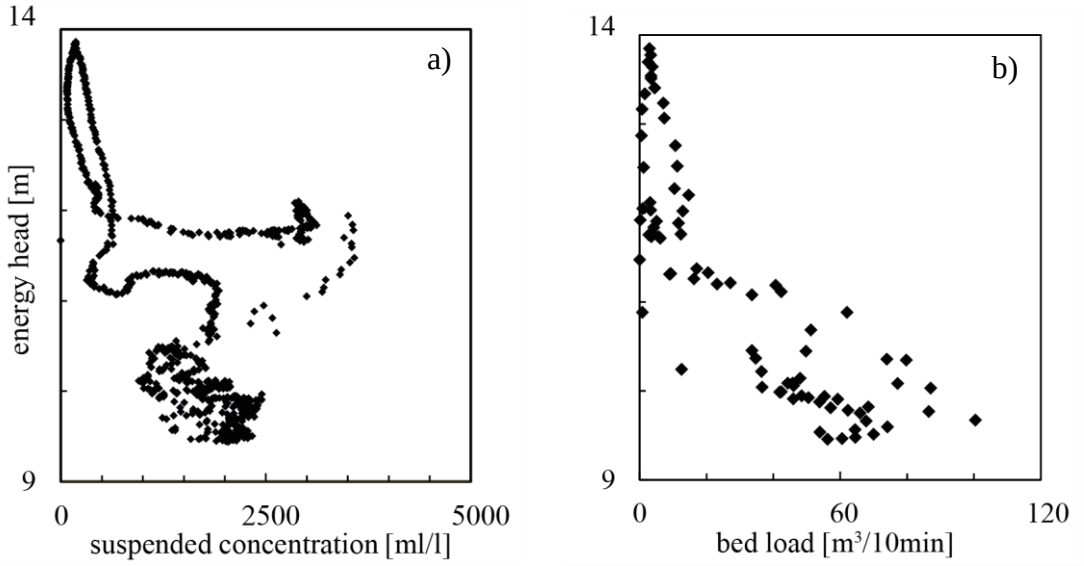

Figure 5: a) Suspended sediment concentration, and b) bed load transport rate depending on energy head during operation on 13th August 2014

Furthermore, the geophone system registered unevenly distributed bedload transport in the spanwise direction. Over 90% of the triggered bed load was transported on the orographic right tunnel side and showed an exponential distribution increasing towards the tunnel wall. This phenomenon resulted from the effect of the bend located 100 m upstream. It induces secondary flow currents causing sediment concentration at the inner side of the bend.

During the first three operations the measured bypassed sediment volume varied between 20'000 and 80'000 m^3, but the portion of bed load was insignificant. Consequently, no abrasion was observed. However, during the operation in August 2014 the suspended and the bed load transport mass were considerable and first abrasion traces were observed. Although an abrasion measurement is yet to be done, visual inspections already showed that cast basalt plates suffered from abrasion at the upstream edges while the concrete fields generally experienced comprehensive abrasion following an undulating pattern. However, at the test fields equipped with high alumina cement concrete and ultra-high-performance fiber-reinforced concrete no abrasions were visible.

4.2 Pfaffensprung SBT

In 2012 and 2013 the Pfaffensprung SBT was in operation for 113 and 131 days, respectively and let all test fields suffer from hydroabrasion. Due to the tunnel bend, abrasion occurred more intensely on the orographic right side, especially for the older concrete near the outlet. Furthermore, comparison of the abrasion topography between 2012 and 2013 revealed that the abrasion pattern stayed similar but amplified and damages grew in streamwise direction (Figure 6a and Figure 6b).

The abrasion on the concrete test fields showed an undulating pattern, whereas the abrasion on the granite test fields were concentrated at the lateral joints and upstream edges of the tiles (Hagmann *et al.* 2014). The mean abrasion rates were 2 mm and 14 mm per year while the maximal abrasion rates were 15 and 35 mm per year for granite and concrete, respectively. Note that the maximal abrasion rates are decisive for SBB to define the refurbishment intervals.

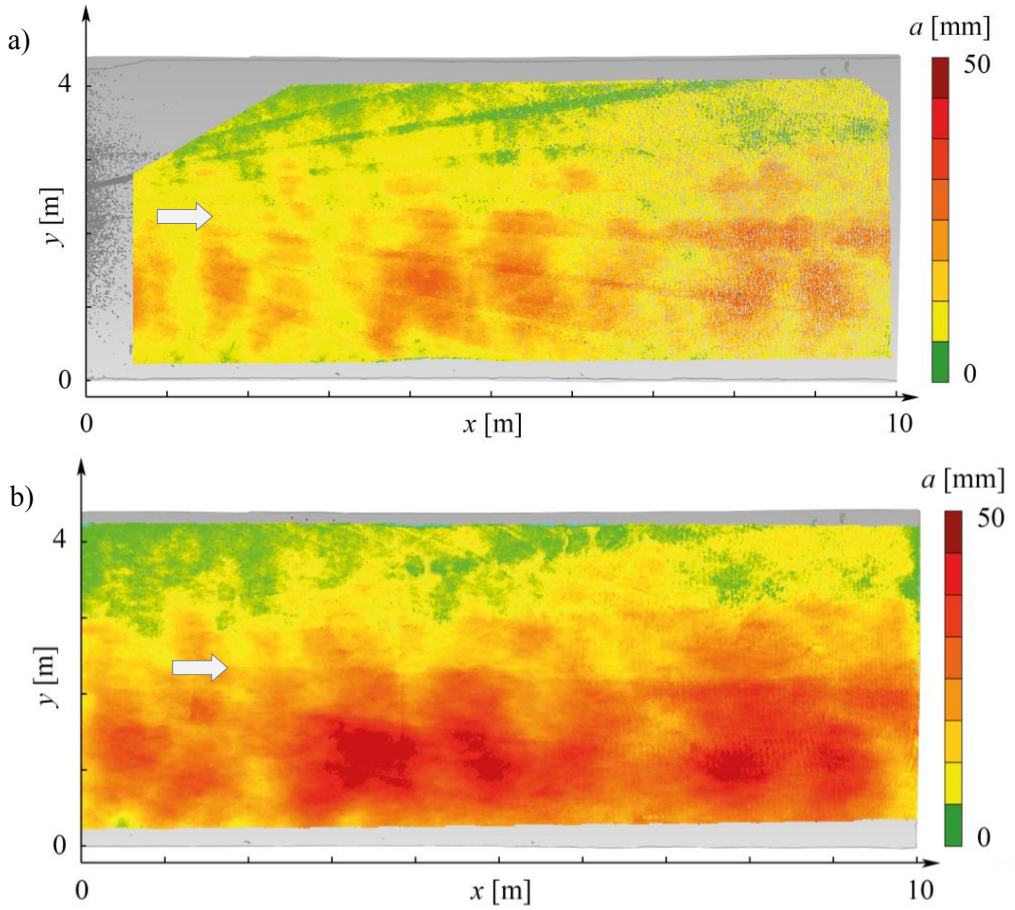

Figure 6: Abrasion of a high strength concrete test field in the Pfaffensprung SBT, a) after one year and b) after two year of operation, flow direction from left to right

4.3 Hydroabrasion drum

The concrete specimens taken from Pfaffensprung SBT were tested using the test drum described in Section 3.3. The tests were done using a mixture of 10 kg of water and 10 kg of steel spheres with a mean diameter of 5 mm. The rotation speed was 17 rotations per minute. Thereby the samples were stressed for 0.5454 s per rotation. The test duration was 58.8 h and the stress duration per sample was 9.09 h causing an abrasion rate of 1.1 mm/h (Figure 7). During the laboratory test a linear correlation between abrasion depth and stress duration was observed confirming former results (Auel 2014). Since the field abrasion was 14 mm per year, this laboratory test was able to reproduce the *in-situ* abrasion depth of a whole season in fast motion within less than 59 hours. Thus this testing procedure seems to be suitable for cross-comparison and determination of hydroabrasion resistance of different materials in respect of future applications. However, this promising result must be confirmed by further investigations.

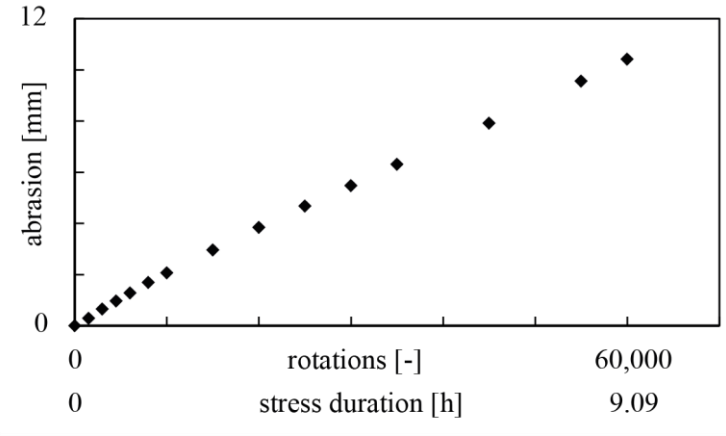

Figure 7: Hydroabrasion drum test results of high-strength concrete implemented in Pfaffensprung SBT; Abrasion as a function of both, stress duration and total number of rotations

5 Design recommendations

Since hydroabrasion is a self-intensifying process, invert irregularities and vulnerabilities or imprecise uneven invert implementation should be avoided or at least minimized in the design and implementation stages. Curves in plan-view should be avoided as sediment transport always occurs on the inner side of the curve due to the development of additional secondary currents. If they are inevitable, invert strengthening along the inner curve should be considered to cope with the increased specific sediment transport rates. Additionally, proper implementation and curing are preconditions for high resistant invert materials. At most sites the grain size distribution covers a large range resulting in a combination of two different particle size-dependent abrasion processes, grinding or impinging. Therefore, it is not possible to equip a facility with an optimum material persisting all operating conditions. Whenever damages appear and surface shows highly irregular pattern and protruding edges, refurbishment should be conducted in order to hinder fast growing damages. Further recommendations may be found in Boes *et al.* (2014).

6 Conclusions

Although hydroabrasion is an omnipresent issue in hydraulic engineering, only few standards or guidelines are available. The operators of facilities facing hydroabrasion wear often test the performance of different materials *in-situ*. However, in many cases even after decades of testing, the optimum lining material is not found. Recent investigations show that laboratory tests using a hydroabrasion drum are suitable to determine the hydroabrasion resistance of lining materials. These results confirm findings of other scientists (Jacobs *et al.* 2001, Kryžanowski *et al.* 2012). However, only a few investigations have been done, thus leaving a knowledge gap concerning the correct simulation of field conditions as well as the transferability of laboratory results to field scale. This requires further experiments.

The present field investigations reveal that monolithic materials exhibit undulating abrasion pattern which sometimes lead to incision channels or pot holes whereas modular materials have weak spots at the joints suffering the highest abrasion rates. Further it is found that hard materials persist suspended sediment. If the dominating abrasion process is caused by saltating particles, materials with high tensile strengths perform better than hard materials prone to brittle fracturing by absorbing the kinetic energy of the impacts. However, force-locked mounting and higher board thickness reduces the risk of fracturing significantly.

Acknowledgement

The authors thank swisselectric research, the Swiss Federal Office of Energy (SFOE), the Swiss association of the cement industry (cemsuisse), the foundation Lombardi Ingegneria, the power company of Zurich (ewz) and the Swiss Federal Railways for supporting the present research project.

References

Auel C. (2014). Flow charachteristics, particle motion and invert abrasion in sediment bypass tunnels. *VAW-Mitteilungen* 229 (R. M. Boes, ed.), ETH Zurich, Switzerland.

Auel C., Boes R., Ziegler T., Oertli C. (2011). Design and construction of the sediment bypass tunnel at Solis. *Hydropower and Dams* (3): 62-66.

Bellmann C. (2012). Deterioration of concrete subjected to hydro-abrasion. *Proc. 9th International PhD Symposium in Civil Engineering*, Karlsruhe Institute of Technology (KIT), Germany.

Bellmann C., Mechtcherine V. (2012). Experimental investigation into the deterioration of ordinary concrete subjected to hydro-abrasion. *Proc. MicroDurability*, PRO83, Amsterdam, Netherland.

Black K., Rosenberg M. (1994). Suspended sand measurements in a turbulent environment: field comparison of optical and pump sampling techniques. *Coastal Engineering* 24 (1): 137-150.

Boes R. M., Auel C., Hagmann M., Albayrak I. (2014). Sediment bypass tunnels to mitigate reservoir sedimentation and restore sediment continuity. *Proc. International Riverflow Conference* (A. J. Schleiss *et al.*, eds.), Lausanne, Switzerland: 221-228.

Bogen J., Møen K. (2001). Bed load measurements with a new passive ultrasonic sensor. *Erosion and Sediment Transport Measurement: Technological and Methodological Advances, International Association of Hydrological Sciences*: 19-21.

Delley P. (1988). Erosionsschäden am Umleitstollen Palagnedra und deren Sanierung ('Erosion damages at bypass tunnel Palagnedra and its rehabilitation'). *Proc. Internationales Symposium über Erosion, Abrasion und Kavitation im Wasserbau*, VAW-Mitteilung 99 (D. Vischer, ed.), VAW, ETH Zurich, Switzerland: 329-352.

Felix D., Albayrak I., Boes R. M. (2013). Laboratory investigation on measuring suspended sediment by portable laser diffractometer (LISST) focusing on particle shape. *Geo-Marine Letters* 33 (6): 485-498.

Gottesfeld A. S., Tunnicliffe J. (2003). Bed load measurements with a passive magnetic induction device. *IAHS-Publication*: 211-221.

Grasso D. A., Jakob A., Spreafico M. (2005). Abschätzung der Schwebstofffrachten mittels zweier Methoden. *Wasser Energie Luft* 99 (3): 273-280.

Habersack H., Haimann M., Kerschbaumsteiner W., Lalk P. (2008). Schwebstoffe im Fließgewässer: Leitfaden zur Erfassung des Schwebstofftransportes ('Suspended sediment in waterscourse: guidline for registration of suspended sediment transport'), Bundesministerium für Land- und Forstwirtschaft, Umwelt und Wasserwirtschaft, Vienna, Austria.

Hagmann M., Albayrak I., Boes R. M. (2012). Reduktion der Hydroabrasion bei Sedimentumleitstollen - In-situ-Verusche zur Optimierung der Abrasionsresistenz ('Reduction of hydroabrasion at sediment bypass tunnels - In-situ experiments to optimize the abrasion resistance'). *Proc. Wasserbausymposium "Wasser - Energie, global denken - lokal handeln"* (G. Zenz, ed.), TU Graz, Austria: 91-97.

Hagmann M., Albayrak I., Boes R. M. (2014). Untersuchung verschleissfester Materialien im Wasserbau mit einer Geschiebtransportüberwachung ('Investigation abrasion resistant materials at hydraulic structures with a bed load monitoring'). *Proc. Internationales Symposium „Wasser- und Flussbau im Alpenraum“*, VAW-Mitteilung 227 (R. M. Boes, ed.), ETH Zurich, Switzerland: 97-106.

Jacobs F., Hagmann M. (2015). Sediment Bypass Tunnel Runcahez: Invert Abrasion 1995-2014. *Proc. First International Workshop on Sediment Bypass Tunnels*, VAW-Mitteilungen 232 (R. M. Boes, ed.), Zurich, Switzerland.

Jacobs F., Winkeler W., Hinkeler F., Volkart P. (2001). Betonabrasion im Wasserbau ('Concrete abrasion at hydraulic structures'). *VAW-Mitteilung*(H.-E. Minor, ed.), ETH Zurich, Switzerland.

Kryžanowski A., Mikoš M., Šušteršič J., Ukrainczyk V., Planinc I. (2012). Testing of concrete abrasion resistance in hydraulic htructures on the Lower Sava River. *Strojniški vestnik-Journal of Mechanical Engineering* 58 (4): 245-254.

Mechtcherine V., Bellmann C., Helbig U., Horlacher H. B., Stamm J. (2012). Nachbildung der Hydroabrasionsbeanspruchung im Laborversuch Teil 1 - Experimentelle Untersuchung zu Schädigungsmechanismen im Beton ('Modeling hydroabrasive stress in the laboratory experiment, part 1 - experimental investigations of damage mechanisms in concrete'). *Bautechnik* 89 (5): 309-319.

Møen K., Bogen J., Zuta J., Ade P., Esbensen K. (2010). Bedload measurement in rivers using passive acoustic sensors. *US Geological Survey Scientific Investigations Report* 5091: 336-351.

Morach S. (2011). Geschiebemessung mittels Geophonen bei hohen Fliessgeschwindigkeiten - Hydraulische Modellversuche ('Bedload transport measurement at high flow velocities - hydraulic model tests'). *Master Thesis*, VAW, ETH Zurich, Switzerland, (unpublished).

Müller B., Walker M. (2015). The Pfaffensprung sediment bypass tunnel: 95 years of experience. *Proc. First International Workshop on Sediment Bypass Tunnels*, VAW-Mitteilungen 231 (R. Boes, ed.), VAW, ETH Zurich, Switzerland.

Nakajima H., Otsubo Y., Omoto Y. (2015). Abrasion and corrective measurement of a sediment bypass system at Asahi Dam. *Proc. First international Workshop on Sediment Bypass Tunnels*, VAW Mitteilungen 232 (R. M. Boes, ed.), ETH Zurich, Switzerland.

Oertli C. (2009). Entlandung des Stausees Solis durch einen Geschiebeumleitstollen. *Wasser Energie Luft* 101. Jahrgang, Heft 1: 5-9.

Oertli C., Auel C. (2015). Solis sediment bypass tunnel: First operation experiences. *Proc. First International Workshop on Sediment Bypass Tunnels*, VAW-Mitteilungen 232 (R. Boes, ed.), VAW, ETH Zurich, Switzerland.

Rickenmann D., McArdell B. W. (2007). Continuous measurement of sediment transport in the Erlenbach stream using piezoelectric bedload impact sensors. *Earth Surface Processes and Landforms* 32 (9): 1362-1378.

Rickenmann D., Turowski J. M., Fritschi B., Klaiber A., Ludwig A. (2012). Bedload transport measurements at the Erlenbach stream with geophones and automated basket samplers. *Earth Surface Processes and Landforms* 37 (9): 1000-1011.

SBZ (1943). Rekonstruktion des Umleittunnels am Pfaffensprung des Kraftwerks Amsteg der SBB. *Schweizerische Bauzeitung* 121: 41-42.

Vischer D., Hager W. H., Casanova C., Joos B., Lier P., Martini O. (1997). Bypass tunnels to prevent reservoir sedimentation. *Proc. 19th ICOLD Congress* Q74 R37, Florence: 605-624.

Wren D., Barkdoll B., Kuhnle R., Derrow R. (2000). Field techniques for suspended-sediment measurement. *Journal of Hydraulic Engineering* 126 (2): 97-104.

Wyss C. R., Rickenmann D., Fritschi B., Weitbrecht V., Boes R. M. (2014). Bedload grain size estimation from the indirect monitoring of bedload transport with Swiss plate geophones at the Erlenbach stream. *Proc. River Flow 2014* (A. Schleiss *et al.*, eds.), Lausanne: 1907-1912.

Authors

Michelle Hagmann (corresponding Author)
Laboratory of Hydraulics, Hydrology and Glaciology (VAW), ETH Zurich
Email: hagmann@vaw.baug.ethz.ch

Dr. Ismail Albayrak
Prof. Dr. R.M. Boes
Laboratory of Hydraulics, Hydrology and Glaciology (VAW), ETH Zurich

May 9-12
Kyoto-Japan
2017

2nd International Workshop on
Sediment Bypass Tunnels

Field calibration of abrasion prediction models for concrete and granite invert linings

Michelle Müller-Hagmann, Ismail Albayrak and Robert M. Boes

Abstract

Hydroabrasive wear is an omnipresent issue at hydraulic structures exposed to high sediment loads and flow velocities, causing considerable refurbishment costs. Its prediction is mandatory for design life estimations and cost-effectiveness analyses. Despite available abrasion prediction models, their applicability to hydraulic structures is scarcely investigated, leaving a lack of knowledge. Therefore, prototype experiments were conducted at several Swiss sediment bypass tunnels and abrasion models were evaluated. The results indicate that the abrasion models are applicable to predict abrasion depth and rate at hydraulic structures. Furthermore, average and material-specific calibration coefficients were determined. The latter significantly reduce the prediction error.

Keywords: invert abrasion, abrasion prediction models, field calibration, 3D laser scan

1 Introduction

Hydraulic structures exposed to mechanical stress caused by sediment-laden flow suffer continuous material loss, i.e. so-called hydroabrasion. This is an important but still not satisfactorily solved issue negatively affecting the cost-effectiveness of hydraulic structures. Most of the existing research studies mainly focus on bedrock incision of rivers as a landscape shaping process, whereas hydroabrasion of concrete and other invert materials such as granite and basalt plates has been less investigated in the past (Ishibashi 1983, Sklar and Dietrich 2004, 2012, Huang and Yuan 2006, Helbig and Horlacher 2007, Lamb *et al.* 2008, 2015, Chatanantavet and Parker 2009, Helbig *et al.* 2012, Auel 2014, Beer and Turowski 2015, Auel *et al.* 2017a). In particular, prototype experiments are rare and the field application of established abrasion models to highly supercritical flows over fixed planar beds of low relative roughness height is questionable. To fill this research gap, prototype tests of various invert materials at Swiss sediment bypass tunnels (SBTs) were conducted in the scope of a PhD research project (Mueller-Hagmann 2017). The obtained data serve for evaluation and enhancement of existing abrasion prediction models, namely the *saltation abrasion model* (SAM) developed by Sklar and Dietrich (2004) and its enhanced version, the *saltation abrasion model Auel* (SAMA) in particular accounting for supercritical flow conditions introduced by Auel *et al.* (2017a).

2 Methodology

Prototype experiments were conducted at the Pfaffensprung, Runcahez and Solis SBTs. The abrasion depths of the test fields were measured using a high resolution 3D-laser scanner and a digital levelling device. The high resolution 3D laser scans performed at Solis SBT resulted in abrasion depths in the range of the measurement accuracy of the device and hence were not used for further analysis. The test fields of the Runcahez SBT were already implemented and monitored in the 1990s in the scope of a former project (Jacobs *et al.* 2001) and hence provide the first long-term prototype hydroabrasion data set to the authors' knowledge (Jacobs and Hagmann 2015). Furthermore, additional data provided by different SBT operators were also included for the evaluation of abrasion prediction models.

2.1 Test site Pfaffensprung SBT

The Pfaffensprung SBT is located in the Swiss Alps, featuring a catchment area of 390 km^2. The tunnel is 280 m long, has a design discharge capacity of 220 m^3/s in free-surface flow and is in operation around 100 to 200 days per year on average (Mueller and Walker 2015, Mueller-Hagmann 2017). Four different 4.4 m wide and 0.3 m thick test fields were implemented in the SBT during the refurbishment works in the low flow winter seasons 2011/12 and 2012/13. Two 10 m long test fields were located at the outlet of the tunnel (location 1 in Figure 1) and another two 20 m long test fields were located in the bend section of the tunnel (location 2 in Figure 1). At both test locations, granite and concrete test fields were implemented. Their properties, namely compression strength f_c, splitting tensile strength f_t and Young's modulus Y_M are listed in Table 1.

Between 2012 and 2015, the SBT was in operation for 118 days per year on average. The mean discharge, flow velocity and annual bedload mass amounted to $Q = 68$ m^3/s, $U = 10.3$ m/s and 350 000 ton, respectively.

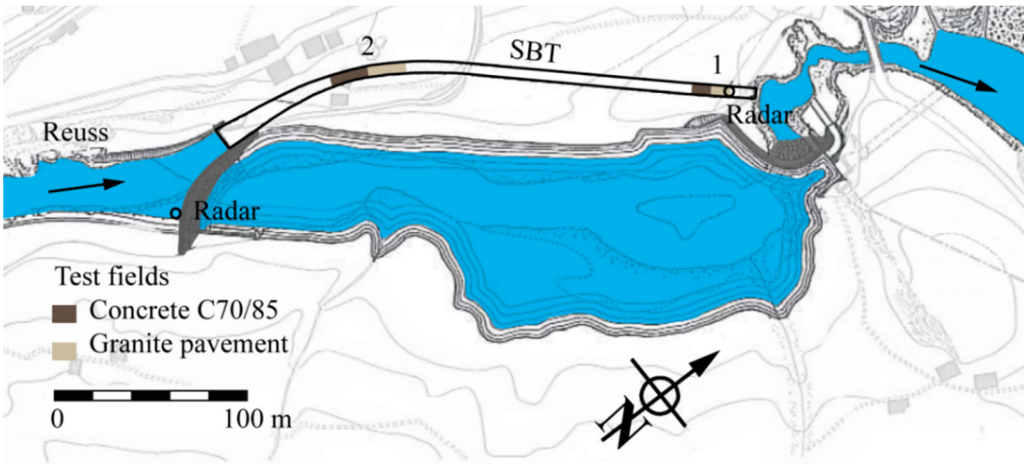

Figure 1: Overview of the Pfaffensprung SBT with the test fields 1 and 2 and the discharge measurement devices (radars)

Table 1: Properties of the implemented material at the Pfaffensprung SBT

Material (Implementation)		f_c [MPa]	f_t [MPa]	Y_M [GPa]
Concrete C1 (2011/12), location 1	C1	108 ± 2 (n=9)	11.3 ± 0.3	38.6
Concrete C2 (2012/13), location 2	C2	78 ± 2 (n=18)	11.2 ± 1.1	34.6
Granite G1 (2011/12), location 1	G1	260 ± 20	10 ± 2	59.0
Granite G2 (2012/13), location 2	G2	260 ± 20	10 ± 2	59.0

2.2 Test site Runcahez SBT

The Runcahez SBT is located in the Eastern Alps of Switzerland, featuring a direct catchment area of 55.6 km^2. The tunnel is 570 m long, has a design discharge capacity of 110 m^3/s in free-surface flow and is in operation during flood events for a few days per year. In 1995, five test fields were implemented along the tunnel section after the acceleration section and bend (Figure 2). They are 10 m long, 3.8 m wide and 30 cm thick and consist of different concrete mixtures. Their material properties are listed in Table 2. Note that the roller compacted concrete (RCC) suffered massive abrasion and required a replacement after Jacobs *et al.'s* (2001) investigation. More details on the Runcahez SBT are given by Jacobs *et al.* (2001), Jacobs and Hagmann (2015) and Mueller-Hagmann (2017).

Since hydraulic conditions were monitored neither in the river nor in the SBT, the discharges were derived from the hydrograph of a nearby gauging station located 3.5 km upstream. Between 1995 and 2014, the annual SBT operation duration of 1.5 days was assumed and accordingly the estimated mean discharge, flow velocity and annual bedload mass amounted to Q = 60 m^3/s, U = 7.6 m/s and 13'900 ton, respectively.

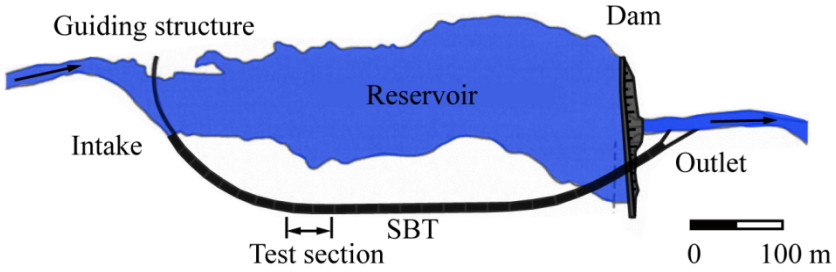

Figure 2: Overview of Runcahez SBT and location of the test section

Table 2: Properties of invert materials implemented at Runcahez SBT (Jacobs *et al.* 2001)

Material	Silica fume concrete (SC)	High performance concrete (HPC)	Steel fiber reinforced concrete (SF)	Roller compacted concrete (RCC)	Polymer concrete (PC)
f_c [MPa]	85.9 ± 3.1	76.7 ± 2.0	95.9 ± 2.3	55.7 ± 4.6	66.8 ± 3.0
f_t [MPa]	8.5 ±2.1	7.1 ± 3.0	8.3 ± 2.0	6.1 ± 1.0	11.7 ± 1.0
Y_M [GPa]	54.1 ± 2.8	52.7 ± 4.1	52.1 ± 2.7	49.7 ± 1.3	16.3 ± 1.3

2.3 Abrasion prediction models

Sklar and Dietrich (2004) investigated bedrock abrasion caused by bedload particles in saltation motion by using an in-house designed abrasion mill device. They developed the following physically-based model for the estimation of the bedrock incision rate, the so-called *saltation abrasion model* (SAM):

$$A_r = \frac{Y_M}{k_v f_t^2} \cdot \frac{W_{im}^2}{L_p} \cdot q_s \cdot \left(1 - \frac{q_s}{q_s^*}\right) \quad [1]$$

where A_r = abrasion rate [m/s], k_v = dimensionless abrasion coefficient, W_{im} = vertical particle impact velocity, L_p = particle hop length, q_s = specific gravimetric bedload transport rate per unit width [kg/(s·m)] and q_s^* = specific bedload transport capacity per unit width [kg/(s·m)]. Explanations of each term in the equation are given by and Sklar and Dietrich (2004) and Auel *et al.* (2017b).

Sklar and Dietrich (2004) re-arranged Eq. [1] by applying particle saltation trajectory equations resulting in:

$$A_r = 0.08 g (s-1) \frac{Y_M}{k_v f_t^2} \cdot q_s \cdot \left(1 - \frac{q_s}{q_s^*}\right) \left(\frac{\theta}{\theta_c} - 1\right)^{-0.5} \left(1 - \left(\frac{U_*}{V_s}\right)^2\right)^{1.5} \quad [2]$$

where g = gravitation acceleration, $s = \rho_s/\rho$ = ratio of solid (index s) to water density, θ = non-dimensional shear stress = $R_h S/[(s-1)D]$, R_h = hydraulic radius, S = energy slope, D = characteristic particle diameter, θ_c = critical shear stress for incipient motion and V_s = particle settling velocity. Within this study, $\theta_c = 0.005$ was chosen for particle motion over plane fixed beds according to Auel *et al.* (2017c). The specific gravimetric bed load transport capacity per unit width was determined according to Smart and Jäggi (1983) using:

$$q_s^* = 7.35 \cdot q \frac{\rho_s}{(s-1)} \left(\frac{d_{90}}{d_{30}}\right)^{0.2} S^{1.6} \left(\frac{1.5\theta - \theta_c}{1.5\theta}\right) \quad [3]$$

Note that the term $(d_{90}/d_{30})^{0.2}$ is typically taken as 1.05 (Smart and Jäggi 1983). Since the bedload transport capacity q_s^* of SBTs is typically significantly larger than the effective bedload transport rate q_s of the inflowing river, the term $(1-q_s/q_s^*)$ in Eqs. [1] and [2], expressing the so-called cover effect, tends to unity and therefore is sometimes neglected. The cover effect describes the complete cover of a fixed bed by sediment, resulting in an effective transport of particles over a movable bed. Depending on the boundary conditions, temporary bed cover may occur, particularly in pressurized inflow conditions (Boes *et al.* 2017), so that the cover effect in the abrasion models term should not generally be skipped.

Sklar and Dietrich (2004) assumed a constant Young's modulus of $Y_M = 50$ GPa and determined k_v for a range of invert materials. They proposed $k_v = 10^6$ while the effective

values ranged from 1.3×10^6 to 9.1×10^6 (Sklar and Dietrich 2004, 2012). This parameter is a function of material properties and therefore requires additional investigations for an appropriate determination (Whipple and Tucker 1999, Momber 2014, Beer and Turowski 2015, Lamb *et al.* 2015, Oertli and Auel 2015, Small *et al.* 2015).

Auel *et al.* (2017a) revised Eq. [1] based on data obtained from their experimental investigation on bedload particle motion and supercritical flow characteristics over a fixed planar bed simulating the flow conditions in SBTs. They proposed:

$$A_r = \frac{Y_M}{k_v f_t^2} \cdot \frac{(s-1)g}{230} q_s \left(1 - \frac{q_s}{q_s^*}\right) \quad [4]$$

This model is herein called *saltation abrasion model Auel* (SAMA) and the effective Young's moduli are accounted for in contrast to Sklar and Dietrich (2004).

3 Results

The k_v values were determined from the present prototype results and additional SBT data applying (I) SAM, i.e. constant Young's modulus, (II) SAM using the corresponding Young's moduli of the materials, denoted as SAM* and (III) SAMA. Figure 3 shows the k_v values as a function of the corresponding splitting tensile strength. For all three approaches a considerable scatter of more than an order of magnitude is observed. The scatter of k_v values from SAM is higher than that from SAM*, while the k_v values from SAMA scatter the least in particular by neglecting the outlines. This result indicates that SAMA is more suitable than SAM and SAM* for the abrasion prediction in high-speed flows.

The k_v values marked with red circles in Figure 3 are from the other SBTs, where no systematic and precise measurements were conducted and many input parameters were based on estimations or assumptions. As a result, the k_v values determined for those SBTs have high uncertainties and highly scatter. Apart from that, the k_v values for concrete from the Pfaffensprung and Runcahez SBTs are in good agreement. Only the value for the polymer concrete is relatively low due to the effect of polymer causing higher ductility and hence different abrasion behavior. Therefore, this data point is not considered in the data evaluation (marked by a green circle in Figure 3a, b and c).

For the remaining concrete test fields, the mean abrasion coefficients of $k_v = 1.35\cdot10^6\pm5\%$, $1.2\cdot10^6\pm30\%$, and $2.0\cdot10^5\pm5\%$ are determined for SAM, SAM* and SAMA, respectively. These values are in good agreement with both Sklar and Dietrich (2001), who proposed $k_v = 10^6$ for the SAM, and with Auel *et al*. (2017a), who found $k_v = 1.9\times10^5$ with SAMA for the concrete invert at the Asahi SBT (Figure 3a, b and c).

Cross comparison of k_v values of different materials revealed significant differences. The k_v values for the granite at the Pfaffensprung SBT is about one order of magnitude higher

than the proposed mean k_v values. This result is against theory on which all three models are based. Despite this fact, the present k_v value for granite is still in a good agreement with Sklar and Dietrich's (2001, 2004) laboratory results where k_v^* for hard rock such as limestone, quartzite and granite was $k_v^* \approx 10^7$. Regarding the steel lining at Mud Mountain SBT, the k_v values are about one order of magnitude below the proposed values. Since these models were developed for brittle materials, deviations for ductile materials such as steel are expected. While brittle materials exhibit a linear elastic stress-strain behavior, the stress-strain curve of ductile materials is linear elasto-plastic. Hence, its fracture energy representing the abrasion resistance is considerable underestimated, which results in lower k_v values.

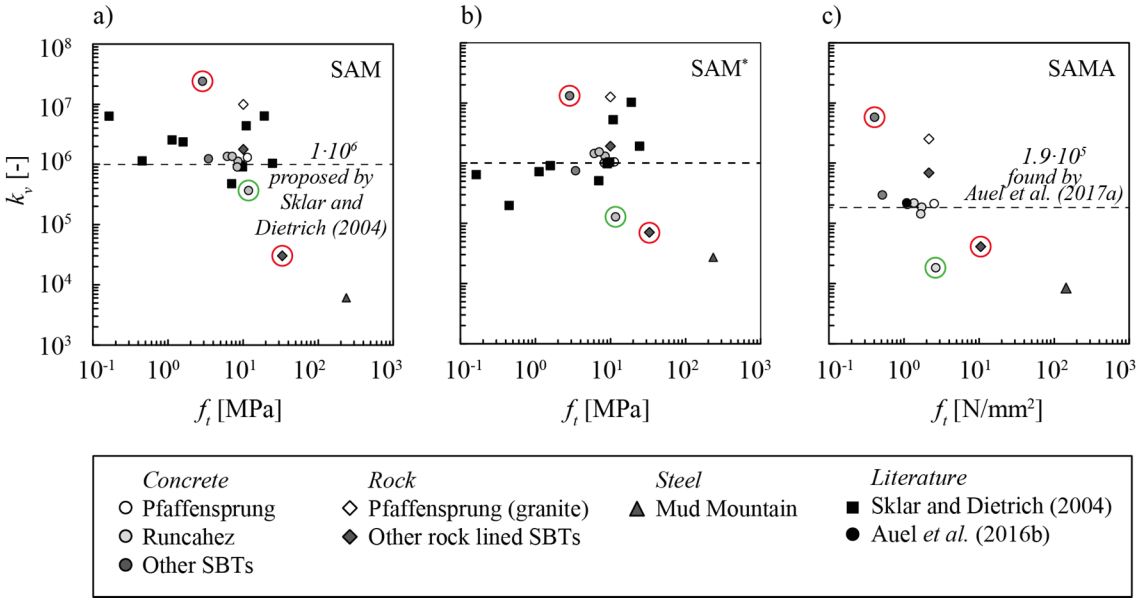

Figure 3: k_v for a) SAM, b) SAM* and c) SAMA as a function of tensile strength; green circle denotes polymer concrete data not further accounted for; red circle denotes data based on uncertain input parameters

4 Conclusions and Outlook

Invert abrasion rates can be predicted by applying various available abrasion models. Amongst others, both saltation abrasion models SAM introduced by Sklar and Dietrich (2004) and SAMA developed by Auel *et al*. (2017a) are applicable for the hydroabrasion prediction in SBTs. The present results indicate that the former should be applied for subcritical flow conditions, while the latter is suitable in particular for the supercritical flow conditions and sediment transport characteristics existing in SBTs.

The prediction accuracy of both models depends on the choice of the abrasion coefficient k_v. In contrast to theory, k_v was found to depend on invert material properties such as strength and hence should be selected accordingly.

Both SAM and SAMA do not account for the effect of sediment shape and hardness, which have a strong influence on the abrasion rate (Sklar and Dietrich 2004). By including these parameters, the prediction accuracy of the models may be additionally enhanced. Therefore, further investigations including the mineral composition and the grain shape of the sediment are recommended.

Acknowledgement

The authors thank *swisselectric research*, the electric utility of Zurich *ewz*, the Swiss Federal Office of Energy SFOE, the association of the Swiss cement industry *Cemsuisse*, the Lombardi Foundation, the Swiss Federal Railways *SBB* and the *Kraftwerke Vorderrhein / axpo* for supporting the research project financially or with in-house efforts along the field measurements. This project is embedded into the framework of the Swiss Competence Center of Energy Research – Supply of Electricity (SCCER-SoE).

References

Auel, C., Albayrak, I., Sumi, T., Boes, R. M. (2017a). Sediment transport in high-speed flows over a fixed bed: 2. Particle impacts and abrasion prediction. *Earth Surface Processes and Landforms*, DOI: 10.1002/esp.4132.

Auel, C., Thene, J. R., Müller-Hagmann, M., Albayrak, I., Boes, R. M. (2017b). Abrasion prediction at Mud Mountain sediment bypass tunnel. *Proc. 2ed International Workshop on Sediment bypass tunnels* (T. Sumi ed.), Kyoto, Japan.

Auel, C., Albayrak, I., Sumi, T., Boes, R. M. (2017c). Sediment transport in high-speed flows over a fixed bed: 1. Particle dynamics. *Earth Surface Processes and Landforms*, DOI: 10.1002/esp.4128..

Beer, A. R., Turowski, J. M. (2015). Bedload transport controls bedrock erosion under sediment-starved conditions. *Earth Surface Dynamics* 3: 291-309.

Boes, R.M., Beck, C., Lutz, N., Lais A., Albayrak, I. (2017). Hydraulics of water, air-water and sediment flow in downstream-controlled sediment bypass tunnels. *Proc. 2nd Intl. Workshop on Sediment Bypass Tunnels*, Kyoto, Japan.

Helbig, U., Horlacher, H.-B. (2007). Ein Approximationsverfahren zur rechnerischen Bestimmung des Hydroabrasionsverschleisses an überströmten Betonoberflächen ('Approximation method for the determination of hydroabrasive wear on overflown concrete surfaces'). *Bautechnik* 84 (12): 854-861.

Helbig, U., Horlacher, H., Stamm, J., Bellmann, C., Butler, M., Mechtcherine, V. (2012). Nachbildung der Hydroabrasionsbeanspruchung im Laborversuch Teil 2 - Korrelation mit Verschleisswerten und Prognoseansätze ('Laboratory reproduction of hydroabraison part 2 - correlation with abrasion rates and prediction models'). *Bautechnik* 89 (5): 320-330.

Huang, X.-B., Yuan, Y.-Z. (2006). Mechanism and prediction of material abrasion in high-velocity sediment-laden flow. *Journal of Hydrodynamics*, Ser. B 18 (6): 760-764.

Ishibashi, T. (1983). Hydraulic study on protection for erosion of sediment flush equipments of dams. *Civil Society* 334 (6): 103-112 (in Japanese).

Jacobs, F., Winkeler, W., Hinkeler, F., Volkart, P. (2001). Betonabrasion im Wasserbau ('Concrete abrasion at hydraulic structures'). *VAW-Mitteilung* 168 (H.-E. Minor, ed.), ETH Zurich, Switzerland.

Jacobs, F., Hagmann, M. (2015). Sediment Bypass Tunnel Runcahez: Invert Abrasion 1995-2014. Proc. First International Workshop on Sediment Bypass Tunnels, *VAW-Mitteilungen* 232 (R. M. Boes, ed.), Zurich, Switzerland: 211-222.

Lamb, M. P., Dietrich, W. E., Sklar, L. S. (2008). A model for fluvial bedrock incision by impacting suspended and bed load sediment. *Journal of Geophysical Research-Earth Surface* 113 (F3).

Lamb, M. P., Finnegan, N. J., Scheingross, J. S., Sklar, L. S. (2015). New insights into the mechanics of fluvial bedrock erosion through flume experiments and theory. *Geomorphology* (244): 33-55.

Momber, A. W. (2014). Effects of target material properties on solid particle erosion of geomaterials at different impingement velocities. *Wear* 319 (1): 69-83.

Mueller, B., Walker, M. (2015). The Pfaffensprung sediment bypass tunnel: 95 years of experience. *Proc. First International Workshop on Sediment Bypass Tunnels*, VAW-Mitteilungen 232 (R. Boes, ed.), VAW, ETH Zurich, Switzerland: 247-258.

Mueller-Hagmann, M. (2017). Hydroabrasion by high-speed sediment-laden flows in sediment bypass tunnels (tentative title). *VAW-Mitteilungen* 239 (R. M. Boes, ed.), ETH Zurich, Switzerland: (in preparation).

Oertli, C., Auel, C. (2015). Solis sediment bypass tunnel: First operation experiences. *Proc. First International Workshop on Sediment Bypass Tunnels*, VAW-Mitteilungen 232 (R. Boes, ed.), VAW, ETH Zurich, Switzerland: 223-234.

Sklar, L. S., Dietrich, W. E. (2004). A mechanistic model for river incision into bedrock by saltating bed load. Water Resources Research 40 (6).Boes, R.M., Minor, H.-E. (2002). Hydraulic Design of Stepped Spillways for RCC Dams. *Hydropower & Dams,* 9(3), 87-91.

Sklar, L. S., Dietrich, W. E. (2012). Correction to "A mechanistic model for river incision into bedrock by saltating bed load". *Water Resources Research* 48 (6).

Small, E. E., Blom, T., Hancock, G. S., Hynek, B. M., Wobus, C. W. (2015). Variability of rock erodibility in bedrock‐floored stream channels based on abrasion mill experiments. *Journal of Geophysical Research: Earth Surface* 120 (8): 1455-1469.

Smart, G. M., Jaeggi, M. N. R. (1983). Sedimenttransport in steilen Gerinnen ('Sediment transport in steep channels'). *VAW-Mitteilung* 64 (D. Vischer, ed.), VAW, ETH Zürich, Switzerland.

Whipple, K. X., Tucker, G. E. (1999). Dynamics of the stream-power river incision model: Implications for height limits of mountain ranges, landscape response timescales, and research needs. *Journal of Geophysical Research-Solid Earth* 104 (B8): 17661-17674.

Authors

Michelle Mueller-Hagmann (corresponding Author)
Ismail Albayrak
Robert Michael Boes
Laboratory of Hydraulics, Hydrology and Glaciology (VAW), ETH Zurich, Switzerland

Email: mueller-hagmann@vaw.baug.ethz.ch